AD-A112 042 SRI INTERNATIONAL MENLO PARK CA F/G 20/3
NOVEL EDDYCURRENT PROBE DEVELOPMENT.(U)
DEC 81 A J BAHR, J P WATJEN F33615-80-C-5025
UNCLASSIFIED AFWAL-TR-81-4159 NL

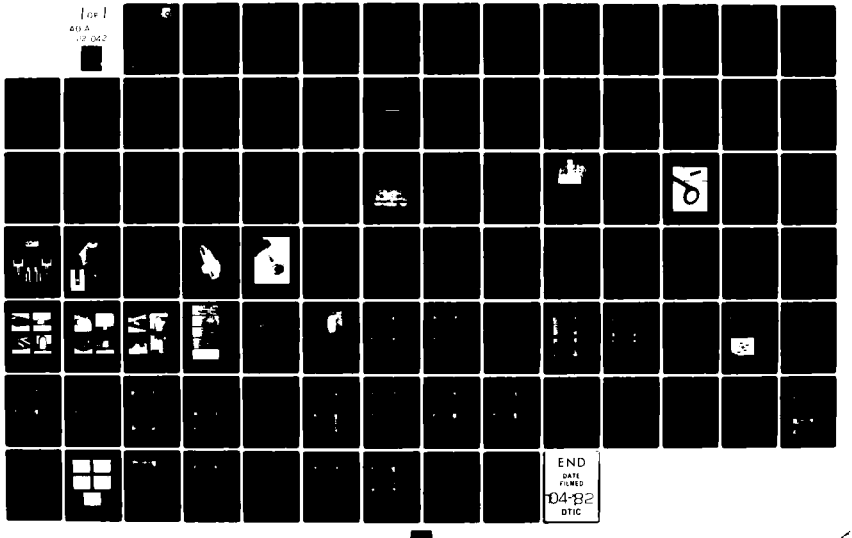

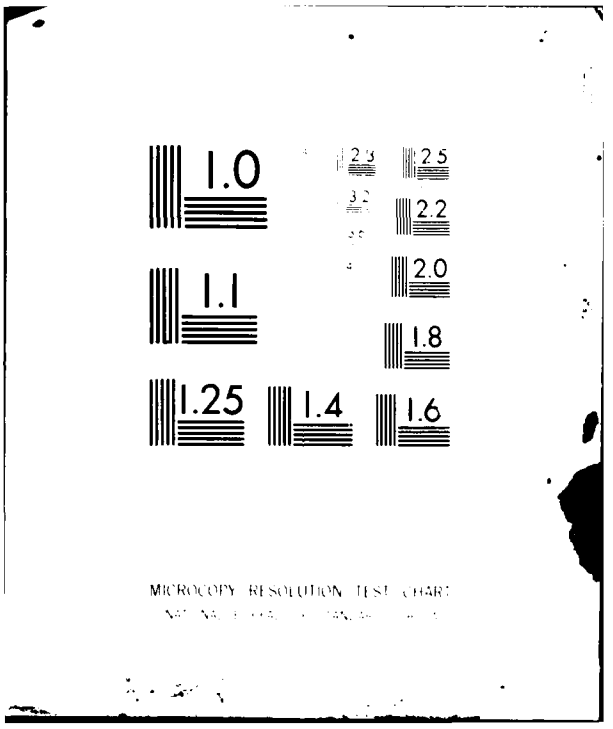
1.0
2.5
2.2
2.0
1.8
1.25
1.4
1.6
MICROCOPY RESOLUTION TEST CHART

AFWAL-TR-81-4159

(12)

NOVEL EDDY-CURRENT PROBE DEVELOPMENT

Alfred J. Bahr John P. Watjen

SRI International
333 Ravenswood Avenue
Menlo Park, California 94025

December 1981

Final Report for Period July 1980 to August 1981

APPROVED FOR PUBLIC RELEASE; DISTRIBUTION UNLIMITED

MATERIALS LABORATORY
AIR FORCE WRIGHT AERONAUTICAL LABORATORIES
AIR FORCE SYSTEMS COMMAND
WRIGHT-PATTERSON AIR FORCE BASE, OHIO 45433

NOTICE

When Government drawings, specifications, or other data are used for any purpose other than in connection with a definitely related Government procurement operation, the United States Government thereby incurs no responsibility nor any obligation whatsoever; and the fact that the government may have formulated, furnished, or in any way supplied the said drawings, specifications, or other data, is not to be regarded by implication or otherwise as in any manner licensing the holder or any other person or corporation, or conveying any rights or permission to manufacture use, or sell any patented invention that may in any way be related thereto.

This report has been reviewed by the Office of Public Affairs (ASD/PA) and is releasable to the National Technical Information Service (NTIS). At NTIS, it will be available to the general public, including foreign nations.

This technical report has been reviewed and is approved for publication.

DALE E. CHIMENTI
Project Engineer

FOR THE COMMANDER

D. M. FORNEY, JR., Chief
Nondestructive Evaluation Branch
Metals and Ceramics Division

If your address has changed, if you wish to be removed from our mailing list, or if the addressee is no longer employed by your organization please notify AFWAL/MLLP, W-PAFB, OH 45433 to help us maintain a current mailing list.

Copies of this report should not be returned unless return is required by security considerations, contractual obligations, or notice on a specific document.

AIR FORCE/56780/8 February 1982 — 430

UNCLASSIFIED

SECURITY CLASSIFICATION OF THIS PAGE (When Data Entered)

REPORT DOCUMENTATION PAGE		READ INSTRUCTIONS BEFORE COMPLETING FORM
1. REPORT NUMBER AFWAL-TR-81-4159	2. GOVT ACCESSION NO. AD-A112042	3. RECIPIENT'S CATALOG NUMBER
4. TITLE (and Subtitle) NOVEL EDDY-CURRENT PROBE DEVELOPMENT		5. TYPE OF REPORT & PERIOD COVERED Final Report covering the period 15 July 1980 to 15 August 1981
		6. PERFORMING ORG. REPORT NUMBER SRI Project 1908
7. AUTHOR(s) A. J. Bahr and J. P. Watjen		8. CONTRACT OR GRANT NUMBER(s) F33615-80-C-5025
9. PERFORMING ORGANIZATION NAME AND ADDRESS SRI International 333 Ravenswood Avenue Menlo Park, CA 94025		10. PROGRAM ELEMENT, PROJECT, TASK AREA & WORK UNIT NUMBERS FY 1457-80-01034
11. CONTROLLING OFFICE NAME AND ADDRESS Materials Laboratory (AFWAL/MLLP) Air Force Wright Aeronatuical Laboratories (AFSC) Wright-Patterson Air Force Base, Ohio 45433		12. REPORT DATE December 1981 13. NO. OF PAGES 96
14. MONITORING AGENCY NAME & ADDRESS (if diff. from Controlling Office)		15. SECURITY CLASS. (of this report) Unclassified 15a. DECLASSIFICATION/DOWNGRADING SCHEDULE

16. DISTRIBUTION STATEMENT (of this report)

Approved for Public Release; Distribution Unlimited.

17. DISTRIBUTION STATEMENT (of the abstract entered in Block 20, if different from report)

18. SUPPLEMENTARY NOTES

19. KEY WORDS (Continue on reverse side if necessary and identify by block number)

Eddy-Current Testing
Nondestructive Evaluation (NDE)
Surface-Crack Detection
Microwaves
Printed Circuits

20. ABSTRACT (Continue on reverse side if necessary and identify by block number)

This report describes the development of two novel eddy-cur.e.. obes that are fabricated using printed-circuit techniques. The objective of thi. work was to develop reproducible, sensitive probes. One of the probes developed is a quarter-wave microstrip resonator that operates at 1 GHz, while the other probe used a broadband printed-circuit coil that can be operated in a frequency range of 10 to 400 MHz. The microwave probe was found to be very sensitive to open flaws, and seems well suited for detecting such flaws in parts that can be

(Abstract continued)

DD FORM 1 JAN 73 1473
EDITION OF 1 NOV 65 IS OBSOLETE

UNCLASSIFIED
SECURITY CLASSIFICATION OF THIS PAGE (When Data Entered)

19. KEY WORDS (Continued)

20 ABSTRACT (Continued)

mechanically scanned past a fixed probe. The sensitivity of the printed-coil probe to open flaws was less than that of the microwave probe, but it was usually better than that exhibited by conventional coil probes. Also, it is easy to fabricate, is reproducible, and is moderately maneuverable.

This report also presents data obtained using a modified floppy-disk head as an eddy-current probe at 100 kHz. This probe showed a high sensitivity to both open and closed flaws and is recommended for further evaluation and development.

Finally, an analysis of an eddy-current system is presented, and the theory describing the interaction between an eddy-current probe and a flaw is reviewed.

A

TABLE OF CONTENTS

LIST OF ILLUSTRATIONS

LIST OF ILLUSTRATIONS (Concluded)

LIST OF TABLES

PREFACE

The work described in this report is part of an ongoing effort at SRI International to develop new and useful nondestructive evaluation techniques. In particular, previous work has concentrated on using microwave techniques to inspect dielectric materials and metallic surfaces. The experience gained in these earlier efforts has proved useful in the development of the eddy-current probes described in this report, particularly the 1-GHz probe.

The authors wish to thank J. H. Hunt for constructing the microwave probes and bridges, R. W. Wanner and L. M. Lumbard for their assistance in mechanical design and construction, and A. C. Phillips for the design of several 100-kHz circuits.

I INTRODUCTION

This report describes work by SRI International to help the U.S. Air Force meet its general requirement for improved nondestructive evaluation (NDE) techniques, which can reduce the operating and support costs of maintaining a fleet of mission-ready aircraft. The development of techniques that will permit the turbine disks in gas turbine engines to be "retired for cause" is of particular interest. These expensive aircraft turbine components now are retired after a predetermined operational life because they may contain fatigue cracks that approach critical size. This retirement time is based on the worst-case fatigue performance exhibited when these disks are tested to destruction by subjecting them to simulated operational duty cycles. Since fatigue lives typically show a scatter of an order of magnitude or more under nominally identical conditions, many of today's components probably are retired after only 10% or less of their potential useful life. This wasteful situation could be eliminated if NDE techniques were developed to separate those components capable of surviving additional duty from those that should be retired from cause.

Eddy-current testing is one form of NDE that holds promise for achieving this goal. In this type of testing, a crack in or near a metal surface is detected by noting the change in resistance and inductance produced in a small coil (probe) that is passed close to and over the crack. In spite of the facts that such eddy-current inspection has been in widespread use for more than 30 years and that a number of different eddy-current instruments are commercially available, there still is a need to improve eddy-current probes. Particular probe characteristics needing improvement are:

- Sensitivity
- Resolution
- Reproducibility.

In addition, improved analytical understanding is needed to optimize probe design and to identify the key parameters required for setting realistic specifications.

One approach to overcoming these deficiencies is to seek and evaluate novel types of eddy-current probes that differ substantially from conventional coil probes. This report describes SRI's efforts to develop one type of novel probe--the printed-circuit (transmission line) probe. We define a printed-circuit probe as one that is fabricated by printed-circuit techniques rather than by winding a fine wire into a coil. Some of the potential advantages we perceive for such printed-circuit probes are:

- Improved reproducibility
- Simpler and cheaper construction than that of previous probes.
- Simpler geometry, thus permitting a more accurate analysis of the probe to be performed.

Printed-circuit techniques are probably best suited for constructing a probe that operates at microwave frequencies because at microwave frequencies transmission-line techniques can be used to implement the required impedance transformations while maintaining a reasonable physical size. Accordingly, the initial effort on this program was devoted to developing a probe that operates at 1 GHz.* We have found such microwave probes to be more sensitive to open surface-breaking cracks than the conventional coil probes that operate at lower frequencies. However, such a high-frequency probe cannot detect a crack that is slightly beneath the metal surface because the corresponding skin depth is so small. Hence, we also constructed and tested a lower-frequency printed-coil probe that can be operated between 10 and 400 MHz. For comparison, eddy-current tests were also conducted at the more conventional frequency of 100 kHz using commercial wound-coil probes and a modified floppy-disk tape head.

---

*In this work, we specifically exclude from consideration the novel ferromagnetic resonance probe currently being developed by Dr. B. A. Auld and his co-workers at Stanford University.

The data presented in this report illustrate the crack-detection sensitivity, resolution, lift-off discrimination, and reproducibility of the microwave and printed-coil probes. Data on the temperature sensitivity of the printed-coil probe are also presented. We conclude from these data that the 1-GHz microwave probe has the highest sensitivity of all the probes to open, surface-breaking flaws such as electrodischarge-machined (EDM) slots, but that the lower-frequency probes are more sensitive to tight fatigue cracks. The intermediate-frequency printed-coil probe appears to offer the best compromise for detecting both open and tight flaws. In addition, the floppy-disk tape head appears very promising for detecting tight fatigue cracks, but further evaluation of this type of probe is required before any definite conclusions can be drawn.

Section II of this report discusses the theoretical design of an eddy-current probe, as well as the design of the overall eddy-current crack-detection system. The experimental results obtained during this program are summarized in Section III; a more detailed discussion of these experimental results is presented in the Appendix. Finally, Section IV presents a summary of the work and our conclusions.

II THEORETICAL MODEL

The modeling of an eddy-current crack-detection system is divided into two parts: One part deals with circuits (i.e., the detection of the signal produced in a probe by a crack), while the other part deals with electromagnetic fields and is concerned with calculating the signal produced by a crack. This section discusses these two aspects of modeling an eddy-current inspection system and their interrelationship.

A. Circuit Model

The general equivalent circuit for an eddy-current inspection system is shown in Figure 1. The system consists of: (1) a probe, (2) an impedance transformer, and (3) a bridge for measuring small changes in the impedance of the probe. The probe is modeled by the impedance of the probe in free space, Z_p, in series with an impedance, Z_c, that is coupled into the probe due to the proximity of a conducting metal surface. It is the coupled impedance, Z_c, that changes in the presence of a crack.

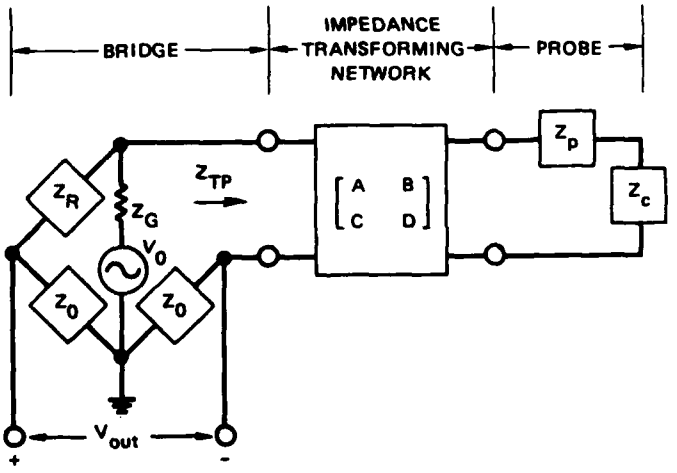

FIGURE 1 EQUIVALENT CIRCUIT OF AN EDDY-CURRENT INSPECTION SYSTEM

The impedance transformer can be modeled in terms of its general circuit parameters, A, B, C, D, or in terms of any other convenient set of circuit parameters. In terms of general circuit parameters, the transformed input impedance of the probe, Z_{TP}, is given by

$$Z_{TP} = \frac{A(Z_p + Z_c) + B}{C(Z_p + Z_c) + D} \quad . \tag{1}$$

The change in input impedance, ΔZ_{TP}, produced by a small change in coupled impedance, ΔZ_c, is therefore given by

$$\frac{\Delta Z_{TP}}{Z_{TP}} = \frac{\Delta Z_c}{[A(Z_p + Z_c) + B][C(Z_p + Z_c) + D]} \quad , \tag{2}$$

where it has been assumed that the matching network is reciprocal, and hence that

$$AD - BC = 1 \quad . \tag{3}$$

As a simple example of matching network, consider an ideal N:1 transformer. In this case, B = C = 0 and A = 1/D = N. Therefore, Eq. (2) becomes

$$\frac{\Delta Z_{TP}}{Z_{TP}} = \frac{\Delta Z_c}{Z_p + Z_c} \quad . \tag{4}$$

Equation (4) is a first-order approximation for a coil probe.

As another example, consider the case where $Z_p + Z_c$ is negligible and the input impedance, Z_{TP}, is determined entirely by losses in the matching network (this is approximately the case for the microwave probe). Then

$$Z_{TP} \simeq B/D \tag{5}$$

and

$$\frac{\Delta Z_{TP}}{Z_{TP}} \simeq \frac{\Delta Z_c}{BD} \quad . \tag{6}$$

Analysis of the bridge circuit shown in Figure 1 shows that the output voltage of the bridge, V_{out}, is given by

$$V_{out} = V_{inc} \frac{Z_0(Z_{TP} - Z_R)}{(Z_0 + Z_R)(Z_0 + Z_{TP})} \quad , \tag{7}$$

where

$$V_{inc} = \frac{V_0}{1 + \frac{Z_G}{Z_0 + Z_{TP}} + \frac{Z_G}{Z_0 + Z_R}} \quad . \tag{8}$$

Clearly, V_{inc} is a maximum when $Z_G = 0$. Also, when the bridge is balanced, $Z_R = Z_{TP}$. If Z_0 is a real impedance, Eq. (7) can be rewritten in terms of the reflection coefficients, Γ_{TP} and Γ_R, as follows:

$$V_{out} = \frac{V_{inc}}{2} (\Gamma_{TP} - \Gamma_R) \quad , \tag{9}$$

where

$$\Gamma_{TP} \triangleq \frac{Z_{TP} - Z_0}{Z_{TP} + Z_0} \tag{10}$$

and

$$\Gamma_R \triangleq \frac{Z_R - Z_0}{Z_R + Z_0} \quad . \tag{11}$$

Equation (9) also results from an analysis of a microwave probe connected to an ideal 180° hybrid. In that analysis one must interpret V_{out} as the amplitude of a wave traveling outward from the difference port of the hybrid toward a matched receiver. The amplitude of the wave incident on the sum port of the hybrid is $V_{inc} = V_0/2$, and the impedance Z_0 is the impedance of the transmission lines that form the four ports of the hybrid.

Note that it is not possible to obtain perfect isolation between the various ports of a practical bridge. For that case, Eq. (9) becomes a much more complicated function of Γ_{TP} and Γ_R. However, in this report, we will consider only an ideal bridge and ignore the slight errors in the theory that result.

Passing the probe over a flaw (or changing the amount of lift-off) produces a change in the output voltage of the bridge that is proportional to the corresponding change in reflection coefficient, $\Delta\Gamma_{TP}$. The quantity $\Delta\Gamma_{TP}$ can be found by differentiating Eq. (10):

$$\Delta\Gamma_{TP} = \left(\frac{2Z_0Z_{TP}}{(Z_{TP} + Z_0)^2}\right)\left(\frac{\Delta Z_{TP}}{Z_{TP}}\right) \quad . \tag{12}$$

Thus, the basic sensitivity of an eddy-current system is determined by the product of two factors: (1) an impedance-match factor

$$F_M \triangleq \frac{2Z_0Z_{TP}}{(Z_{TP} + Z_0)^2} \quad , \tag{13}$$

and (2) a probe-flaw interaction factor

$$F_I \triangleq \frac{\Delta Z_{TP}}{Z_{TP}} \quad . \tag{14}$$

If Z_0 is complex, F_M has a maximum value of 1/2 when $Z_{TP} = Z_0$. If Z_0 is real, F_M has a maximum value of 1 when $Z_{TP} = \pm jZ_0$. This relation is illustrated in Figure 2 for the case of an inductive probe having $Z_{TP}/Z_0 = j(f/f_0)$. In this case, the reduction in sensitivity is severe for $f < f_0$ but only moderate for $f > f_0$.

In general, then, it is desirable to make $|Z_{TP}| = |Z_0|$. Since, for practical reasons, $|Z_0|$ should not be too low or too high (50 Ω is suitable), an impedance transformer will be needed whenever the probe impedance is too low or too high. It should be noted that an impedance transformer is usually not required for a low-frequency coil probe because the number of turns in the coil usually can be chosen to yield a reasonable value for $Z_p + Z_c$.

The equivalent circuit for the matched microwave probe to be described later in this report is shown in Figure 3. At resonance (when ℓ is approximately equal to one-quarter wavelength in the transmission line) the approximate general circuit parameters of the matching network are

$$A = jN_{eff}\pi/(4Q_0) \quad , \tag{15a}$$

$$B = jZ_tN_{eff} \quad , \tag{15b}$$

$$C = j/(N_{eff}Z_t) \quad , \tag{15c}$$

and

$$D = j\pi/(4Q_0N_{eff}) \quad , \tag{15d}$$

where

$$N_{eff}^2 = \frac{(1 - \omega^2 LC_1)}{1 + \frac{C_1}{C_g}} \quad . \tag{16}$$

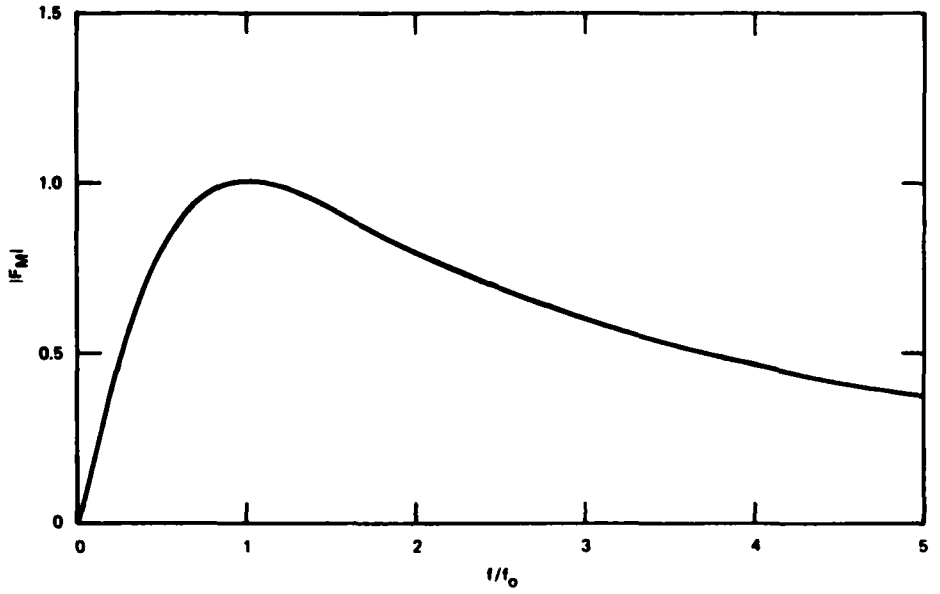

FIGURE 2 VARIATION OF IMPEDANCE-MATCH FACTOR WITH FREQUENCY FOR $Z_{TP}/Z_0 = jf/f_0$

The unloaded Q, Q_0, is related to the attenuation constant, α, in the transmission line by

$$Q_0 = \frac{\pi}{4\alpha\ell} \quad , \tag{17}$$

and Z_t is the characteristic impedance of the transmission-line resonator. The quantity N_{eff}^2 should be chosen to transform the high impedance seen at the input to the transmission-line resonator down to the impedance Z_0.

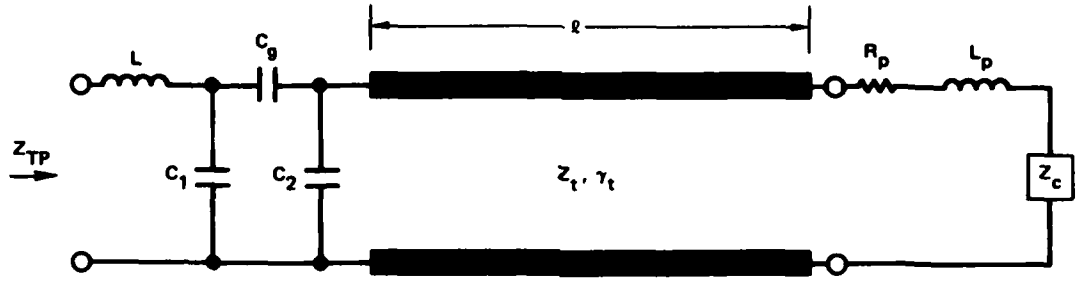

FIGURE 3 EQUIVALENT CIRCUIT OF A MATCHED MICROWAVE EDDY-CURRENT PROBE

Substituting Eqs. (15b) and (15d) into Eq. (6) gives the following result for the interaction factor:

$$F_I^{TL} \simeq -\frac{4Q_0}{\pi}\frac{\Delta Z_c^{TL}}{Z_t} \quad . \tag{18}$$

In summary, Eq. (12) tells us that the sensitivity of the resonant microwave probe whose equivalent circuit is shown in Figure 3 will be maximum when (1) N_{eff} is chosen so that $Z_{TP} = Z_0$, and (2) the ratio Q_0/Z_t is maximum. Condition 1 is relatively easy to achieve in practice. The ratio Q_0/Z_t increases with increasing microstrip width and substrate dielectric constant, as well as with decreasing height of the microstrip above the ground plane. However, the overall probe sensitivity

and resolution will decrease if the microstrip becomes much wider than the crack whose presence is being sought (ΔZ_c decreases). Hence, the microstrip cannot be made too wide, and the height of the microstrip above the ground plane and the dielectric constant are determined by such practical convenience factors as substrate availability and ease of fabrication. The dimensions chosen for the experimental probe (see Figure A-9) were such that $4Q_0/\pi Z_t \simeq 5$. Thus, for the transmission-line probe and microwave hybrid we have

$$\Delta V_{out}^{TL} = \frac{V_{inc}^{TL}}{2} F_M^{TL} F_I^{TL} \simeq \frac{V_0}{4}\left(\frac{1}{2}\right)\left(-5\ \Delta Z_c^{TL}\right) \quad . \tag{19}$$

It is interesting to compare this result with that obtained for a coil probe. A typical coil probe is the Nortec SP-100, which operates at 100 kHz and has an inductance of 100 μH when pressed against a metal plate. For simplicity, we ignore the resistance of the coil. The inductance of the coil can be approximated by the relation

$$L_p + L_c = N^2 F(R) \quad , \tag{20}$$

where N is the number of turns in the coil, and F is a form factor that depends on the average coil radius R.[1]* The number of turns in the Nortec SP-100 probe is 250. Hence, since $L_p + L_c = 100$ μH, we find from Eq. (20) that

$$F(R) \simeq 1.6 \times 10^{-9} \quad . \tag{21}$$

Next, if we interpret ΔZ_c and $Z_p + Z_c$ in Eq. (4) as impedances produced by a single-turn coil, we have

$$F_I^C \simeq \frac{\Delta Z_c^C}{j\omega F(R)} \quad . \tag{22}$$

---

*References are listed at the end of this report.

Finally, if we assume that the generator impedance, Z_G, shown in Figure 1 is zero, and that Z_0 is chosen to be equal to the reactance of the coil, the output voltage of the Wheatstone bridge is

$$\Delta V_{out}^{C} = \frac{V_{inc}^{C}}{2} F_M^C F_I^C \simeq \frac{V_0}{2}(1)(-j1000\ \Delta Z_c^C) \quad . \tag{23}$$

If the Thevenin source voltages, V_0, are adjusted so that V_{inc} is the same for both the coil and transmission-line probes, the ratio of the magnitudes of the output voltages obtained in the two cases is

$$\left| \frac{\Delta V_{out}^{TL}}{\Delta V_{out}^{C}} \right| \simeq \frac{1}{400} \left| \frac{\Delta Z_c^{TL}}{\Delta Z_c^{C}} \right| \quad . \tag{24}$$

Hence, for the microwave transmission-line probe to be more sensitive than the coil probe, we estimate that the magnitude of ΔZ_c^{TL} measured at microwave frequencies must exceed the magnitude of ΔZ_c^C measured at 100 kHz by more than two orders of magnitude. The next section discusses one theoretical approach to calculating ΔZ_c.

B. Field Model

One effective method for calculating ΔZ_c is based on the Lorentz reciprocity theorem.[2] Application of this method to eddy-current problems has been discussed extensively by Auld.[3,4] Basically, the reciprocity theorem relates the change in impedance produced by a flaw to an integral of certain electromagnetic fields on the surface of a volume that encloses the flaw. One form of the mathematical expression for this theorem is

$$\Delta Z_c = \frac{1}{II'} \iint_{S_F} \left[(\tilde{n} \times \vec{E}') \cdot \vec{H} - (\tilde{n} \times \vec{E}) \cdot \vec{H}' \right] dS \quad , \tag{25}$$

where I is the current in the probe, $\tilde{n}$ is a unit vector pointing into the volume enclosed by the surface S_F, $\vec{E}$ is the electric field, and $\vec{H}$ is the magnetic field. The unprimed quantities correspond to the case of no flaw, while the presence of a flaw is indicated by a prime.

It is convenient to rewrite Eq. (25) in terms of the surface impedance, Z_s, where Z_s is defined by the relation

$$\tilde{n} \times \vec{E} = Z_s \vec{H}_t \quad , \tag{26}$$

where $\vec{H}_t$ is the component of $\vec{H}$ tangential to the metal surface.

If the radius of curvature at any point on the surface of the unflawed body is much greater than a skin depth, Z_s is given by the well-known expression

$$Z_s = \frac{1}{Y_s} = (1 + j)R_s \quad , \tag{27}$$

where

$$R_s = \frac{1}{\sigma\delta} \quad . \tag{28}$$

In Eq. (28), σ is the conductivity of the metal and δ is the skin depth.

As a further convenience, we normalize the magnetic fields to the complex amplitude of the applied magnetic field, H_0:

$$\vec{h} = \frac{\vec{H}}{H_0} \quad , \tag{29}$$

and define

$$\vec{m}' = \frac{(\tilde{n} \times \vec{E}')}{H_0} \quad . \tag{30}$$

With these definitions, Eq. (25) becomes

$$\Delta Z_c = \frac{H_0^2}{II'} \iint_{S_F} \left[\left(\vec{m}' \cdot \vec{h} \right) - Z_s \left(\vec{h}_t' \cdot \vec{h}_t \right) \right] dS \quad . \tag{31}$$

Finally, let 2c be a characteristic dimension of the flaw such as crack length, and rewrite Eq. (31) as

$$\Delta Z_c = \left(\frac{2cH_0}{I} \right)^2 \cdot \frac{1}{(2c)^2} \iint_{S_F} \left[\left(\vec{m}' \cdot \vec{h} \right) - Z_s \left(\vec{h}_t' \cdot \vec{h}_t \right) \right] dS \quad , \tag{32}$$

or

$$\Delta Z_c = n_p^2 \cdot \Delta Z_F \quad , \tag{33}$$

where

$$n_p \triangleq \frac{2cH_0}{I} \tag{34}$$

and Z_F can be called the flaw impedance. It has been assumed for simplicity in Eq (32) that $I \simeq I'$. Note that the complex "turns ratio," n_p, is a strong function of lift-off. For example, if the probe is a very thin wire a distance h above a highly conductive surface, we have $n_p \simeq 2c/\pi h$. In addition, the flaw impedance, Z_F, is a function of lift-off because the spatial distribution of the applied fields depends on lift-off.

Equation (32) is a rigorous expression for ΔZ_c; however, its evaluation requires that the fields with and without the flaw be known. Alternatively, from a scattering point of view, one can say that the incident and scattered fields must be known.

Methods for calculating ΔZ_c have been under study for some time and are still a topic of research. Early work by Burrows[5] modeled the flaw as a current dipole and assumed the applied field was uniform. His theory gave good results at low frequencies when the skin depth was large. Later, Dodd[6,7] and his co-workers devised methods for calculating the applied fields produced by practical coils and applied them to computing ΔZ_c for flaws which were small compared to a skin depth.[8,9] These methods made effective use of the computer to solve difference equations or integral equations for the magnetic vector potential.

More recently, Kincaid and his co-workers[10,11] used the finite-element method to calculate applied (incident) fields. They also extended Burrows' theory to permit the calculation of scattering from an ellipsoidal flaw of moderate size with respect to a skin depth. In this case, the incident field was assumed to vary linearly with depth into the material, which led to a representation for the scattering from the flaw as a sum of dipolar and quadrupolar components. This method of combining numerical analysis with classical scattering theory has the advantage of providing considerable physical understanding of the interaction between the eddy-currents and the flaw, and, in particular, provides a method of inversion, namely determining flaw parameters from the eddy-current response.

It is, of course, possible in principle to use finite-element modeling to compute both the incident and scattered fields. However, this approach can lead to considerable computer expense since a separate calculation is required for each change in the flaw parameters. On the other hand, finite-element modeling is applicable to materials that exhibit magnetic nonlinearities,[12] whereas other methods are not. Lord[13] has used finite-element modeling to analyze certain eddy-current phenomena associated with the inspection of steam-generator tubing.

All of the work mentioned above has involved the assumption that the frequency is low enough so that displacement currents in free space can be neglected. This assumption cannot be made at high microwave frequencies.

Bahr[14,15] has analyzed the case of microwave eddy-current interaction with a rectangular open slot in a conducting material under the assumption that skin-effect losses can be neglected. He further assumes that the incident fields are uniform. If the slot length is much less than a free-space wavelength, the result of this analysis is the expression

$$\Delta Z_F \simeq j\eta_0 \left(\frac{\pi^3}{128}\right) k\Delta u \tanh\left(\frac{\pi a}{2c}\right) \quad , \tag{35}$$

where η_0 is the intrinsic impedance of free space (= 120π), Δu is the slot width, $2c$ is the slot length, a is the slot depth, and k is 2π divided by the free-space wavelength. This result was obtained by expanding the fields in the slot in rectangular-waveguide modes.

Plots of $|\Delta Z_F|$ as a function of $k\Delta u$ are shown in Figure 4 for several values of a/c. We see that ΔZ_F increases linearly with depth for small values of a/c, but that this rate of increase diminishes rapidly as a/c approaches unity. This behavior is simply due to the fact that the evanescent fields excited in the slot cannot penetrate to the botton of a deep slot.

It is important to note that this analysis predicts that ΔZ_F approaches zero as the slot closes. Since conventional eddy-current probes which operate at lower frequencies can detect tight cracks (if such cracks are not conductively short-circuited), it is clear that this theory is inadequate for predicting low-frequency eddy-current effects. However, the theory should be fairly accurate for microwave frequencies where the skin depth is very small and displacement currents are significant.

One improvement in the mode-expansion theory just discussed would be to include the effects of a finite skin depth (i.e., finite conductivity). However, the inclusion of finite conductivity complicates the analysis of a three-dimensional slot considerably because the transverse electric (TE) and transverse magnetic (TM) waveguide modes become coupled. An alternative to the model analysis approach that appears more tractable when finite conductivity is included is to seek analytic solutions for the flow

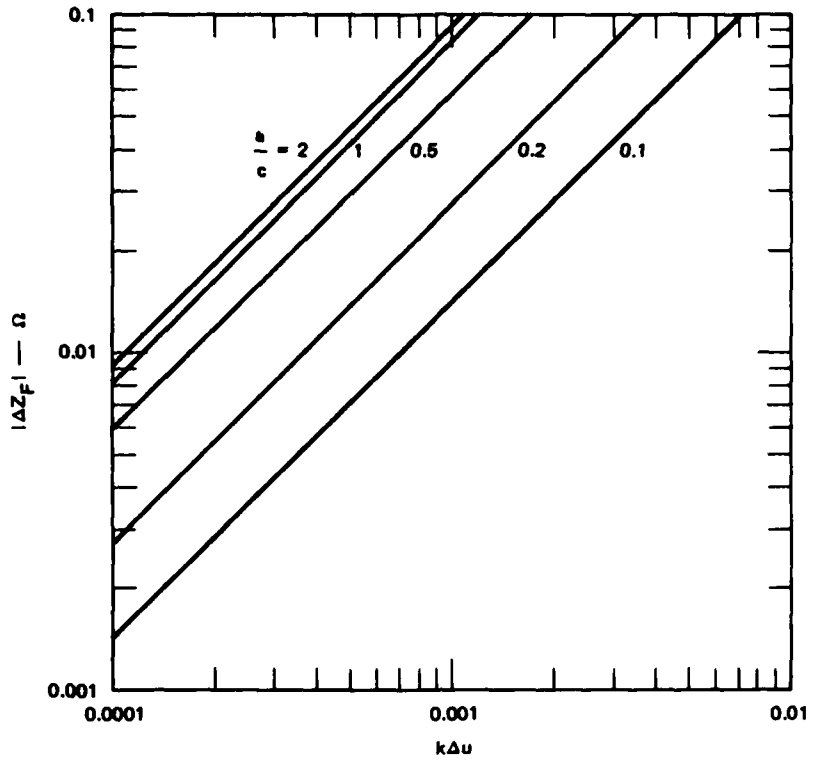

FIGURE 4 THEORETICAL CHANGE IN SLOT IMPEDANCE AS A FUNCTION OF NORMALIZED SLOT WIDTH AND SLOT DEPTH

of eddy-currents around flaws. Beissner et al[16] and Dover et al[17] have shown that such solutions can be obtained by analogy with the solution for the hydrodynamic flow of an incompressible, non-viscous fluid. Auld et al[18] have described how such solutions can be combined with the reciprocity theorem to yield analytic solutions for ΔZ_c. Assuming a uniform incident field, H_0, they derive[19] the following expressions for ΔZ_c of a half-penny-shaped slot:

$\underline{a/\delta << 1}$

$$\Delta Z_c = \left(\frac{2aH_0}{I}\right)^2 (j/\sigma a)\left[\frac{4}{3}\left(\frac{a}{\delta}\right)^2\right] \quad , \tag{36}$$

$\underline{a/\delta >> 1}$

$$\Delta Z_c = \left(\frac{2aH_0}{I}\right)^2 \frac{1}{\sigma a}\left\{(1+j)\frac{\bar{a}}{\delta}\left[1 - \frac{\Delta u}{3\bar{a}}\right] + j\frac{\Delta u}{a}\cdot\frac{a\bar{a}}{\delta^2}\right\} \quad , \tag{37}$$

where $\bar{a} = 0.288a$. Here, as before, a is the slot depth (i.e., the slot radius for the half-penny shape) and δ is the skin depth.

Equation (36) shows that the change in flaw impedance is entirely inductive for $a/\delta << 1$. For $a/\delta >> 1$, Eq. (37) shows that the change in flaw impedance is the sum of two different types of terms: The first term can be called a skin-effect (or internal) impedance, and is just the impedance presented to a strip of current one skin-depth deep that travels around the slot; the second term can be called an external impedance, which, for slot depths of less than a quarter wavelength, is an inductive reactance associated with energy storage in the slot. The skin-effect impedance is composed of equal real and imaginary parts and increases as the square root of frequency, while the external inductive reactance increases linearly with frequency. Hence, at high frequencies the external reactance will dominate the skin-effect impedance, provided the slot is open.

The behavior of the flaw impedance as a function of a/δ and $\Delta u/a$ is shown in Figure 5. In this figure, the real part of the flaw impedance is designated R_F, and the imaginary part X_F. It can be seen that, for relative slot openings, $\Delta u/a$, between 0.01 and 0.1, the external reactance begins to dominate the flaw impedance when $a/\delta \gtrsim 100$ (assuming a is held constant).

As a specific example, we use numbers that correspond to the aluminum sample B-3 that was inspected during the experimental portion of this program (see the Appendix). For this case, $2c = 4.6$ mm, $\Delta u \simeq 0$, and $\sigma = 3.54 \times 10^4$ mho/mm. Assuming $a = c$, we find that $a/\delta \simeq 8.6$ at 100 kHz and that $a/\delta \simeq 860$ at 1 GHz. If we assume that $2aH_0/I$ is roughly the same for the 1-kHz (coil) and 1-GHz (transmission-line) probes, then Eq. (37) shows that Z_c^{TL} is 100 times as large as Z_c^C. Referring back to Eq. (24), we would therefore expect the 1-GHz transmission-line probe to exhibit the same order of sensitivity to this particular tight crack as the 100-kHz coil probe. This is, in fact, what was observed experimentally (see Table 2). On the other hand, as soon as the crack or slot opens,

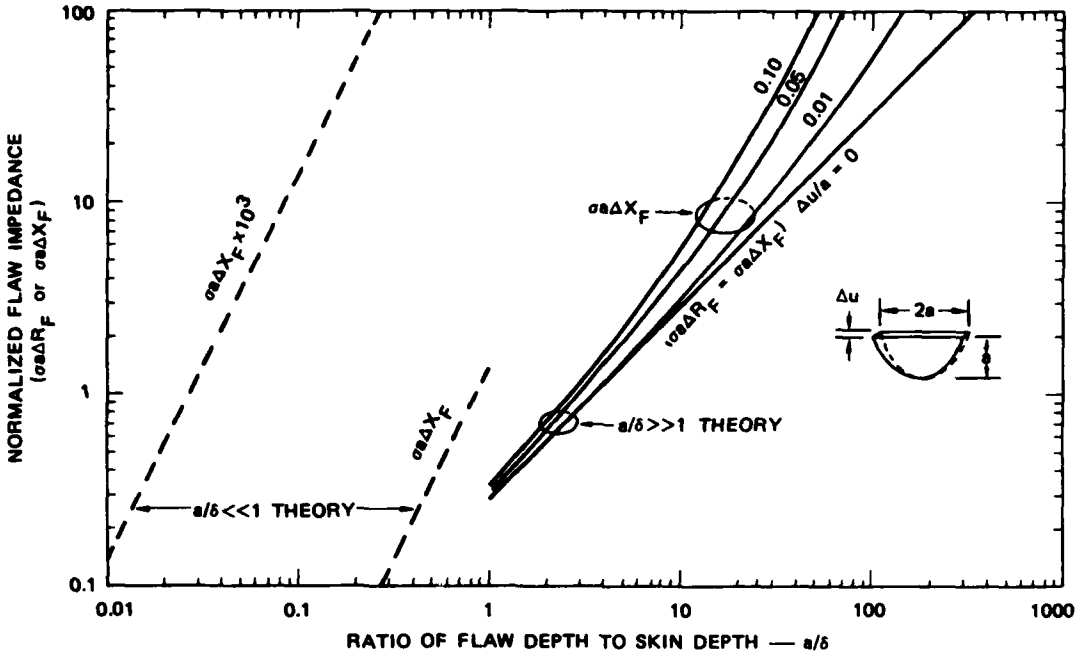

FIGURE 5 FLAW IMPEDANCE FOR A HALF-PENNY SLOT VERSUS RATIO OF FLAW DEPTH TO SKIN DEPTH

we would expect that the sensitivity of the microwave probe to this type of flaw should increase dramatically over that of a lower-frequency coil probe. Again, this is what we observed.

Thus it appears that the simplified theory represented by Eq. (37) is in qualitative agreement with experiment. To obtain better quantitative agreement, the theory must be modified to take into account such features of realistic eddy-current testing as nonuniform excitation fields and irregular flaw shapes.

III EXPERIMENTAL EVALUATION

A. Introduction

The objective of this program is to develop novel eddy-current inspection probes that exhibit high sensitivity to surface-connected flaws, low signal response to extraneous parameters (such as lift-off), and good response reproducibility. In an effort to achieve these objectives, both theoretical and practical considerations led us to investigate three types of probes, each of which operates at widely separated frequencies. Where practical, the probes were configured in a differential arrangement to minimize sensitivity to extraneous parameters. Two of the three probes were fabricated using photolithographic techniques in an effort to achieve economical reproducibility.

The first approach taken in this development was to use a narrowband resonant probe (for high sensitivity) that operated at 1 GHz and which was fabricated using photolithographic techniques. The second approach utilized a broadband nonresonant printed-circuit coil, also fabricated using photolithographic techniques, and which could be operated between 10 to 400 MHz. The third approach utilized a conventional coil wound on a ferrite core (Nortronic H803019 floppy-disk head), the purpose of the ferrite core being to concentrate and guide the magnetic field generated by the probe. This probe operated in the vicinity of 100 kHz.

The performance of the various probes was evaluated by using each probe to scan a variety of open and closed surface-connected flaws in flat metal plates. Commercial coil-type probes (Nortec SP-100, SP/DP-100, and DP-64) that operated at 100 kHz were used to provide performance-level references against which the experimental probes' performances were compared. The most promising experimental probes also were configured as bolt-hole probes and used to scan a small open flaw (EDM slot) on the inner surface of a titanium annular ring.

The various commercial and experimental probes, the flaws that were examined, and the performance of the probes are described in more detail in the Appendix.

The printed-coil probe was found to exhibit the best overall sensitivity to both open and closed surface-connected flaws. Its reproducibility was evaluated by building five such probes and measuring the variability in the responses of the five probes to the EDM slot in the titanium annular ring. The variation of flaw response with changes in temperature was also measured for a single printed-coil probe. In addition, two microwave probes were compared for reproducibility of flaw response.

B. Experimental Arrangement

The experimental arrangement used for comparing the RF and 100-kHz probes is shown schematically in Figure 6. The RF portion consists of an RF source (10 MHz to 1 GHz) and a 100-kHz source which are mixed to produce a coherent single-sideband (SSB) signal. The SSB signal then is amplified and used to drive the RF bridge. Surface-connected flaws that interact with the RF probe disturb the bridge balance, thereby producing a signal at the difference (Δ) port on the bridge. This difference signal then is coherently converted down to 100 kHz, filtered, and processed for display.

The portion of the system that is associated with the 100-kHz probe is made up of a 100-kHz source connected to a driver amplifier having a voltage gain of 10, which in turn drives a 100-kHz bridge. The 100-kHz probe is connected to one arm of the bridge. A detailed schematic diagram of this drive amplifier and bridge arrangement for the Nortec SP-100 probe is shown in Figure 7. A schematic diagram of the bridge used with the floppy-disk probe is shown in Figure 8. Flaws in the sample modify the impedance of the 100-kHz probe and thereby unbalance the bridge. This 100-kHz voltage imbalance then is processed for display in the same way as the signal derived from the RF probe.

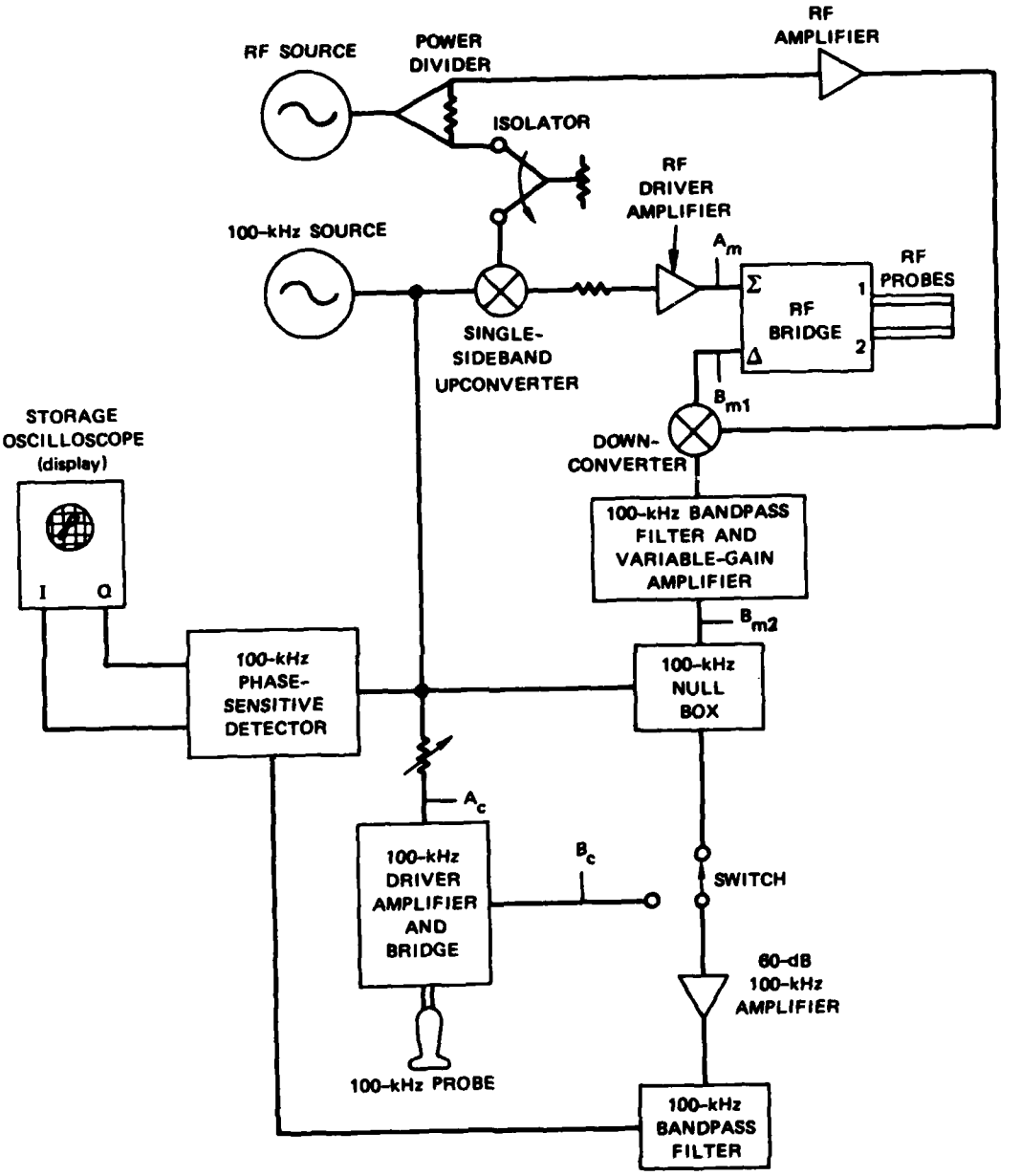

FIGURE 6 EXPERIMENTAL ARRANGEMENT

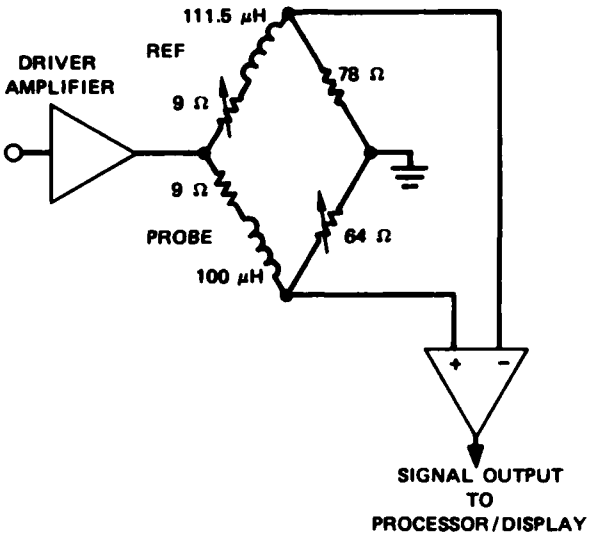

FIGURE 7 SCHEMATIC DIAGRAM OF 100-kHz BRIDGE FOR NORTEC SP-100 PROBE

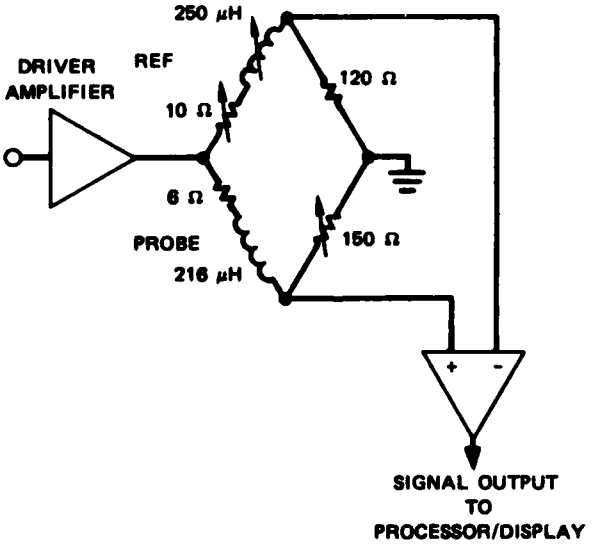

FIGURE 8 SCHEMATIC DIAGRAM OF 100-kHz BRIDGE FOR NORTRONICS H803019 FLOPPY-DISK PROBE

The system is calibrated by measuring the drive voltage, A_m, at the matched input to the RF bridge and setting the drive voltage at the input to the 100-kHz driver, A_c, to $A_m/10$ (because of the internal gain). Having made the input driving signals for the 100-kHz bridge and the RF bridge the same, the next step is to obtain unity voltage gain between the output of the RF bridge, B_{m1}, and the output of the 100-kHz bandpass filter, B_{m2}, by adjusting the variable gain amplifier.

A mechanical stage was used to translate the flat samples past the stationary microwave probe assembly. The stage is mechanically rugged and is mounted on a 1-in.-thick aluminum jig plate that serves as a surface reference plate. Four 0.0001-in.-resolution dial indicators mounted on surface-gage stands were used to measure the heights of the probe and the sample. The mechanical arrangement was rigid enough to provide 0.0002-in. typical repeatability on a scan-to-scan basis. A photograph of this mechanical arrangement is shown in Figure 9.

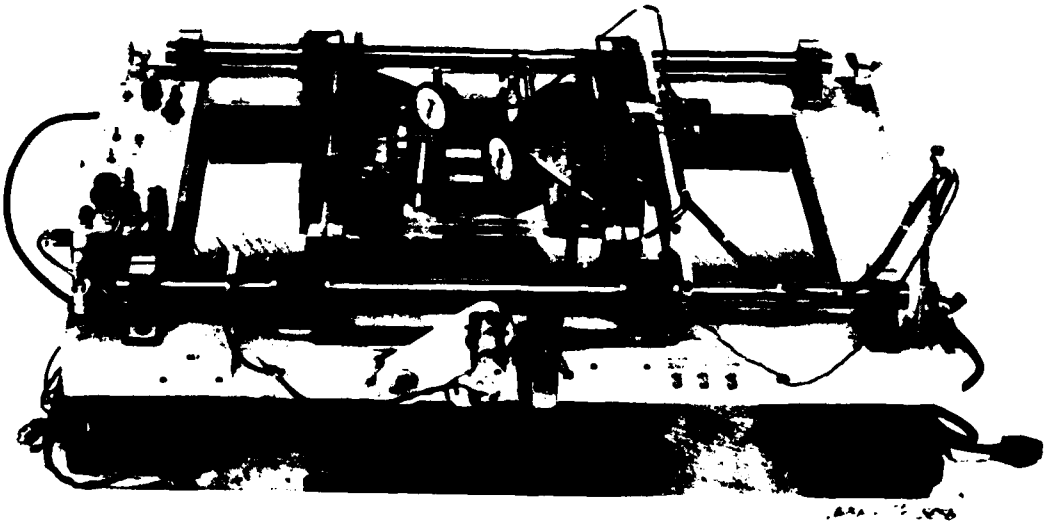

FIGURE 9 MECHANICAL STAGE AND HEIGHT-MEASURING ARRANGEMENT

C. Probe Evaluation Using Surface-Connected Flaws in Flat Plates

1. Microwave Probe

The first probe chosen for evaluation was built using a quarter-wave transmission-line resonator. It consisted of a microstrip line, one quarter-wavelength long at the frequency of interest, which was shorted to the ground plane at one end and capacitively coupled to a 50-Ω microstrip line at the other end. The physical arrangement of this resonator is illustrated in Figure 10. Duroid 5880 was chosen for the substrate material because it is easy to work with, mechanically tough, and has a low dielectric loss tangent. Calculations showed that a Q_0 of 300 should result for a 65-Ω, 1-GHz resonator on a 0.062-in.-thick substrate. A Q_0 of 307 was measured for the shielded resonator in air. Similar agreement was obtained between the calculated and measured values for resonant frequency and input impedance.

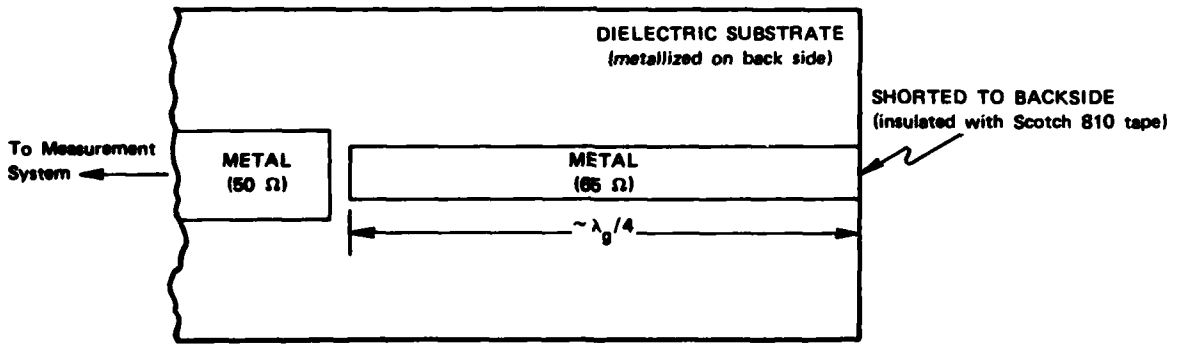

FIGURE 10 QUARTER-WAVE MICROSTRIP RESONATOR

The portion of the transmission-line resonator that passes over the edge of the substrate and is shorted to the ground plane was insulated with 0.002-in.-thick Scotch 810 tape. The metal samples were pressed against this insulated portion of the probe, and the resonator's input impedance and resonant frequency were measured again. All three of the samples that were used (stainless steel, titanium, and aluminum) produced

very nearly the same input impedance and resonant frequency. Based on these measurements, a matching network was designed and incorporated into two probes of the same design. The equivalent circuit for a single matching network and probe is shown in Figure 3. These two probes were integrated with the specially designed microwave bridge shown in Figure 11, which then formed the differential probe assembly shown in Figure 12. The separation between the two probes in this assembly was 0.25 in. The tuning screws on the resonator shields seen in the figure are used to balance the bridge, and the entire assembly can be raised and lowered in a controlled manner. Later, a different probe assembly was designed and built for inspecting holes (see Figure 15), and the candidate probe that appeared most promising based on the flat-plate measurements was tested using the titanium annular ring.

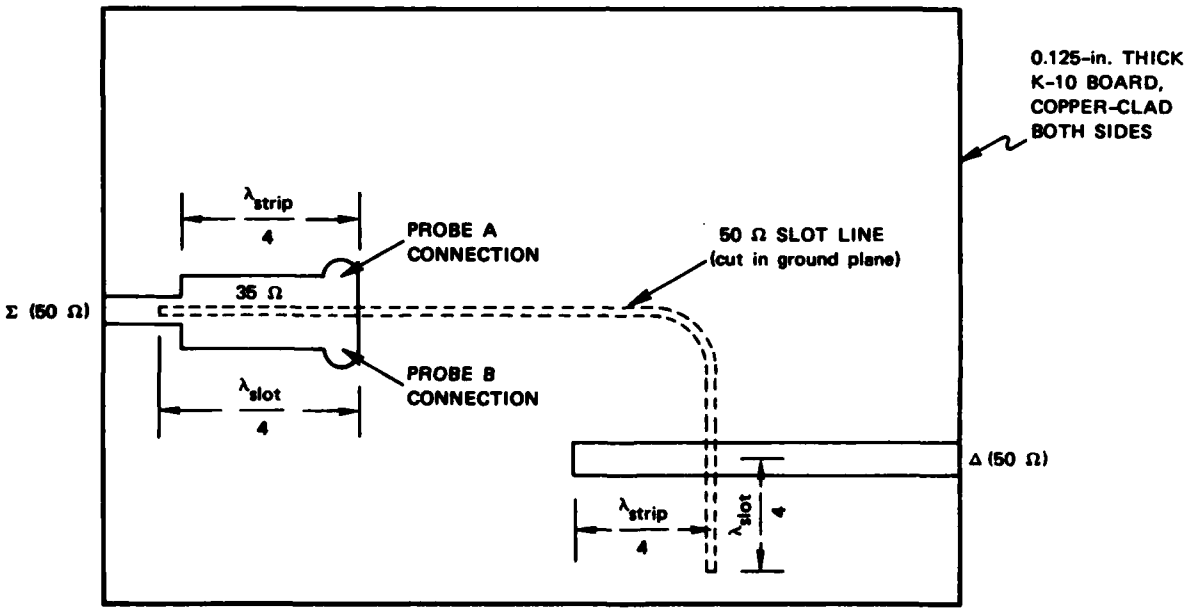

FIGURE 11 CIRCUIT LAYOUT FOR MICROSTRIP -- SLOT-LINE MICROWAVE BRIDGE

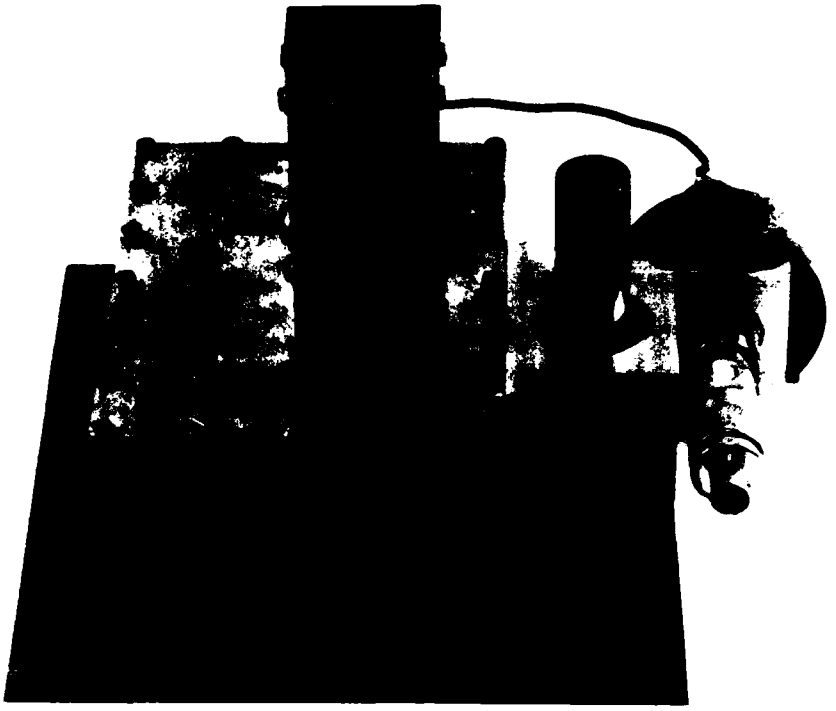

FIGURE 12 DIFFERENTIAL MICROWAVE PROBE ASSEMBLY

During the course of the work, two other microwave probe geometries also were evaluated. These probes were similar to the probe shown in Figure 10 except that each had a slightly different geometry in the region of the probe tip, and so each required a slightly different matching network. A detailed description of these probes is given in the Appendix. After each probe was evaluated and matched, it was integrated with the bridge in the manner described above. The sensitivities of the three differential microwave probes to several surface-connected flaws then were measured and compared to the measured sensitivity of a commercial probe (Nortec Model SP/DP-100) that was used to detect the same flaws.

The most sensitive microwave probe (probe 2) was found to be much more sensitive to open (EDM) slots than the 100-kHz commercial probe. In one case, for example, the sensitivity of the microwave probe to a small slot in titanium was about 45 dB greater than that of the commercial probe. However the microwave probe's sensitivity to closed cracks was a little less than that of the commercial probe.

2. Printed-Coil Probe

This probe consisted of a six-turn planar-spiral inductor that was etched on a low-loss dielectric substrate (Duroid 5880) using photolithographic techniques. The spiral had an outside diameter of 0.1 in. and was connected to the end of a section of 50-Ω semirigid cable. This assembly was enclosed in a plastic handle to facilitate manual scanning of the flat-plate samples. A photograph of this probe is shown in Figure 13. The probe was connected by a short length of flexible 50-Ω coaxial cable to port 1 of the RF bridge shown in Figure 6. A variable reference impedance (a loop of wire) was connected to port 2 of the RF bridge and was adjusted to provide at least 20 dB of common-mode rejection when the probe was positioned at a reference location on the sample to be scanned. Since this probe is non-resonant, it was used to scan the various samples at several different frequencies that ranged between 10 to 400 MHz. Above 400 MHz, increased sensitivity to lift-off prohibited manual scanning. Good sensitivity to both open and closed flaws was observed in the vicinity of 125 MHz. At this frequency, the printed-coil absolute probe was 13 to 35 dB (depending on flaw size) more sensitive to shallow EDM slots than the commercial absolute probe (SP-100). Also, this probe's sensitivity to closed cracks was, depending on the sample, nearly equal to or greater than that of the commercial probe.

3. Floppy-Disk Probe

Although the printed-coil probe did provide better sensitivity to closed cracks than the microwave probe, it was not significantly better than the commercial probe. Part of the problem appears to be that only a small fraction of the magnetic field generated by the printed-coil probe interacts with a small flaw at any given probe position. If a larger fraction of the magnetic field can be directed or focused on the flaw, greater sensitivity can be expected to result. One way to localize the magnetic field at the probe/sample interface is to provide a low-reluctance path for the magnetic fields everywhere except in the vicinity

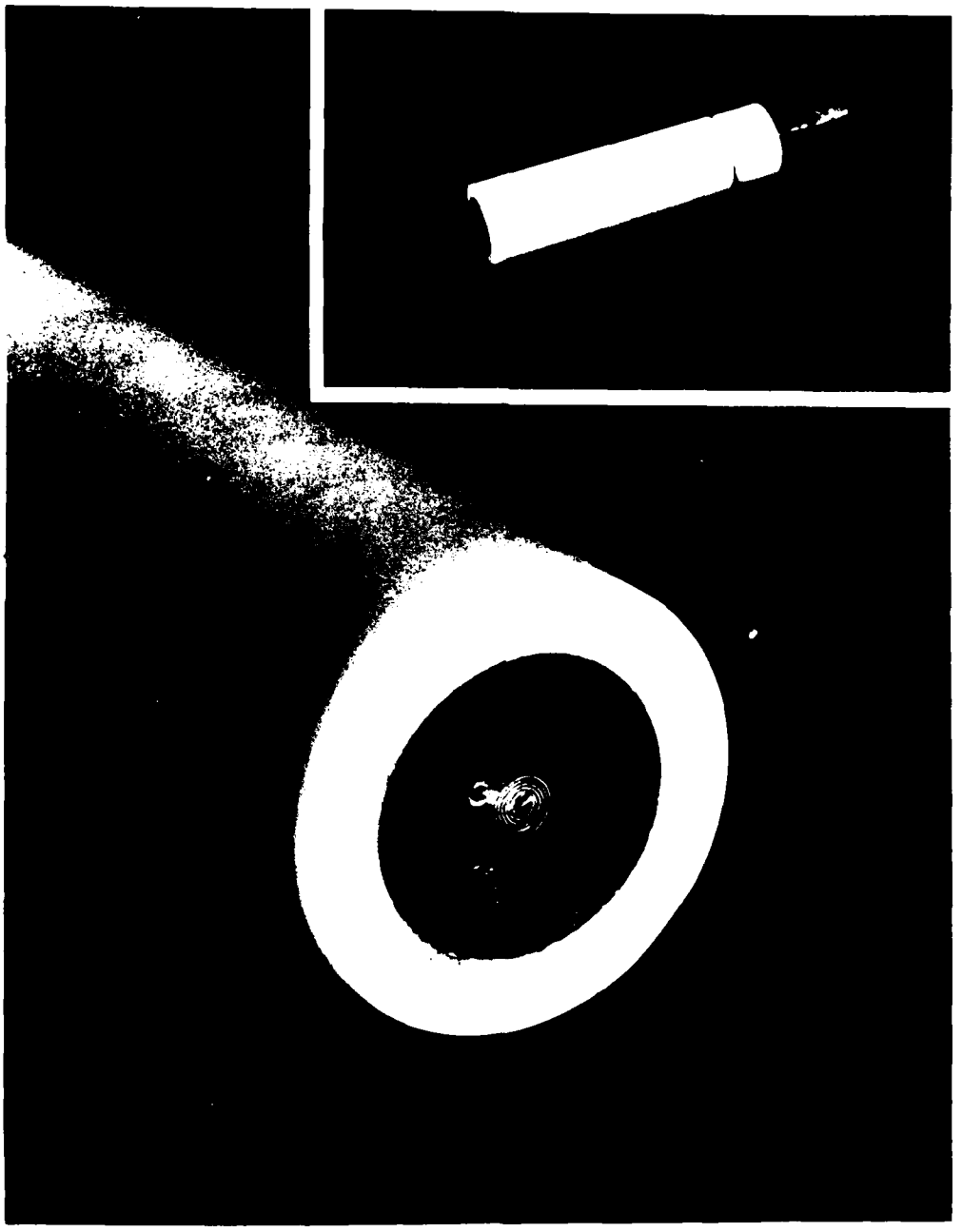

FIGURE 13 PRINTED-COIL PROBE ASSEMBLY

of that interface. Also, we would like to operate in the kilohertz-to-megahertz frequency range and have a nonconducting probe surface so that the probe could rest directly on the sample without the need for an insulating barrier (thus maximizing probe-to-sample coupling). A properly designed ferrite core should satisfy these prescribed conditions.

Since a magnetic recording head must also satisfy a number of the same conditions, two commercial floppy-disk heads (Nortronics p/n H80319, button only) were purchased and evaluated in an effort to test the principle described above in a cost-effective manner. These heads had a spherical surface contour and a glass protective coating. A drawing of the floppy-disk head and gap detail is given in Figure 14. To enhance the coupling between the probe and flat samples, one of the heads was ground flat. This grinding also removed the glass coating and allowed the ferrite to come into contact with the sample.

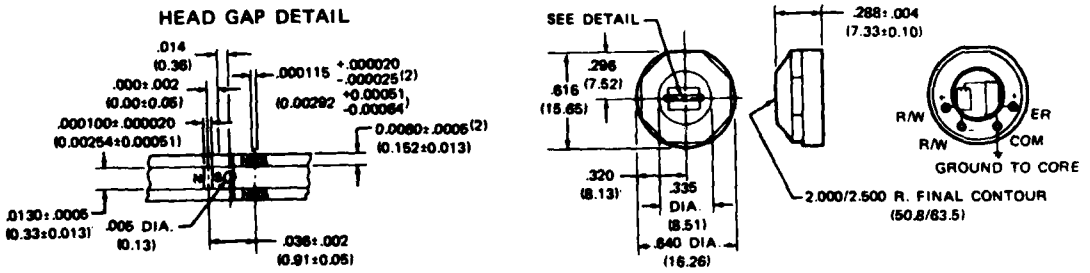

FIGURE 14 DETAILED DRAWING OF FLOPPY-DISK HEAD

This particular tape head is designed to work up to about 250 kHz; therefore, testing the head at 100 kHz presented no problem. The 100-kHz bridge was modified for this purpose, as shown in Figure 8.

Scanning of the flat-plate samples showed that the sensitivity of this probe to closed cracks was 15 to 20 dB better than that of the commercial probe (SP-100), and that its sensitivity to shallow EDM slots was about 9 dB greater.

D. Probe Evaluation Using Titanium Annular Ring

The most promising probe candidates were selected based on their flat-plate flaw-detection performance and were configured as hole-inspection probes. These candidates were: (1) microwave probe 2, (2) the printed-coil probe, and (3) the floppy-disk probe. The flaw to be scanned was a small EDM slot (338 μm long x 156 μm wide x 40 μm deep) located on the surface of a 2.5-cm-diameter hole in a split titanium ring provided by the Air Force. A commercial bolt-hole probe (Nortec DP-64) was intended to be used as a reference for the sensitivity measurements. However, at the signal levels required for comparison purposes, the flaw could not be detected by the commercial probe. The same electrical arrangement was used for the hole inspections as was used for the flat-plate inspections.

1. Microwave Probe

The microwave hole-inspection probe was designed to be used to inspect holes with diameters as small as 1.2 cm. The differential probe assembly was spring loaded about a pivot post (see Figure 12) so it could scan noncircular or eccentric holes. It was necessary to use mechanical scanning to minimize background signals caused by lift-off variations. Photographs of the microwave-hole inspection probe are shown in Figure 15. The metallic surfaces of this probe were insulated from the sample with 0.002-in.-thick Scotch 810 tape.

This probe exhibited a defect sensitivity to the tiny EDM slot of about 1.6 V. Although the phasor flaw response was colinear with the background (lift-off) response, the flaw signal was easy to identify because the flaw produced a rapidly varying bi-polar signal as it was scanned, while the background signal was relatively slowly changing.

2. Printed-Coil Probe

This probe was designed to manually scan the 2.6-cm-diameter hole in the split titanium ring. The copper spiral was insulated from the sample with 0.002-in.-thick Scotch 810 tape. A photograph of this

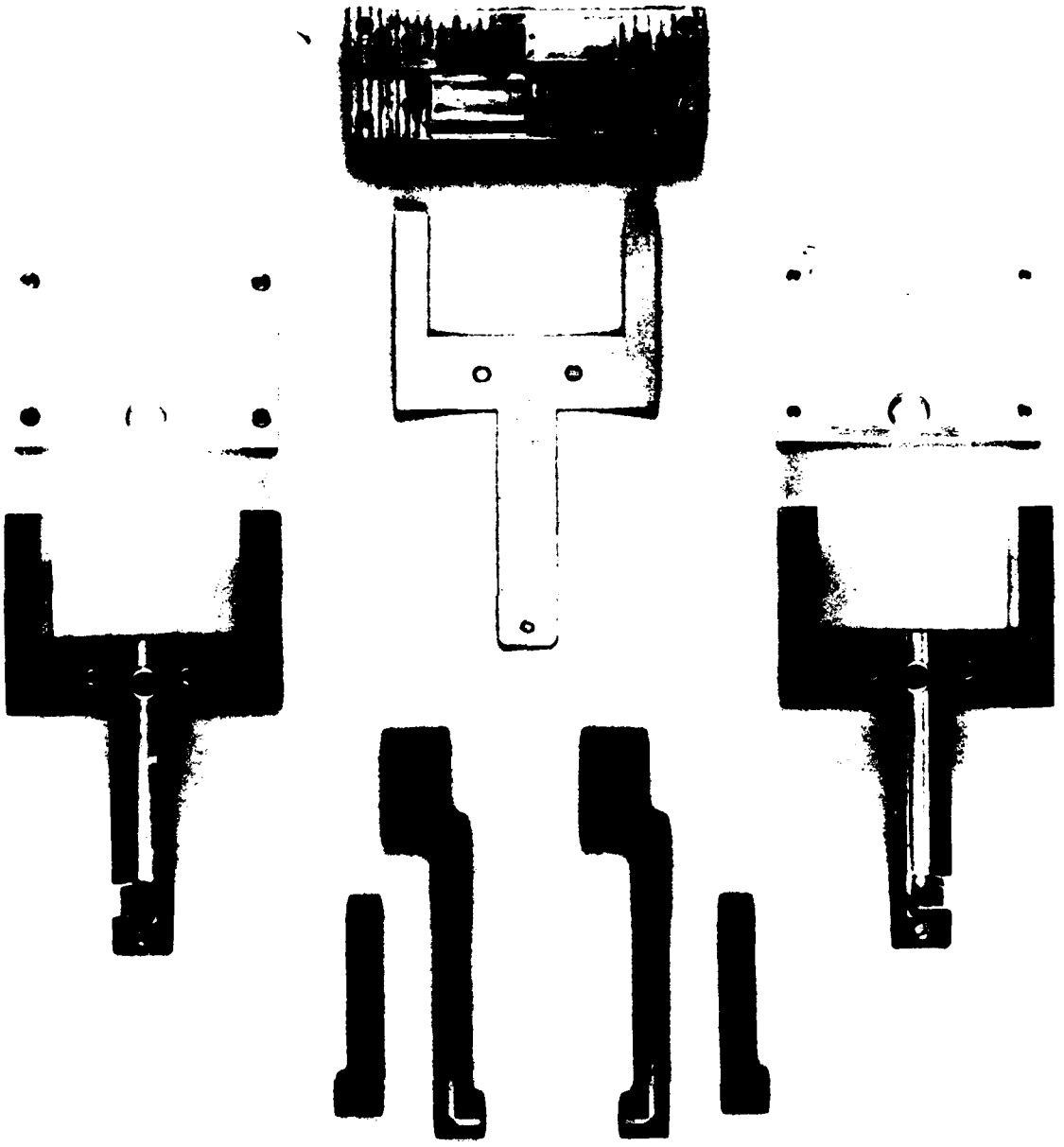

(a) DISASSEMBLED

FIGURE 15 MICROWAVE HOLE-INSPECTION PROBE

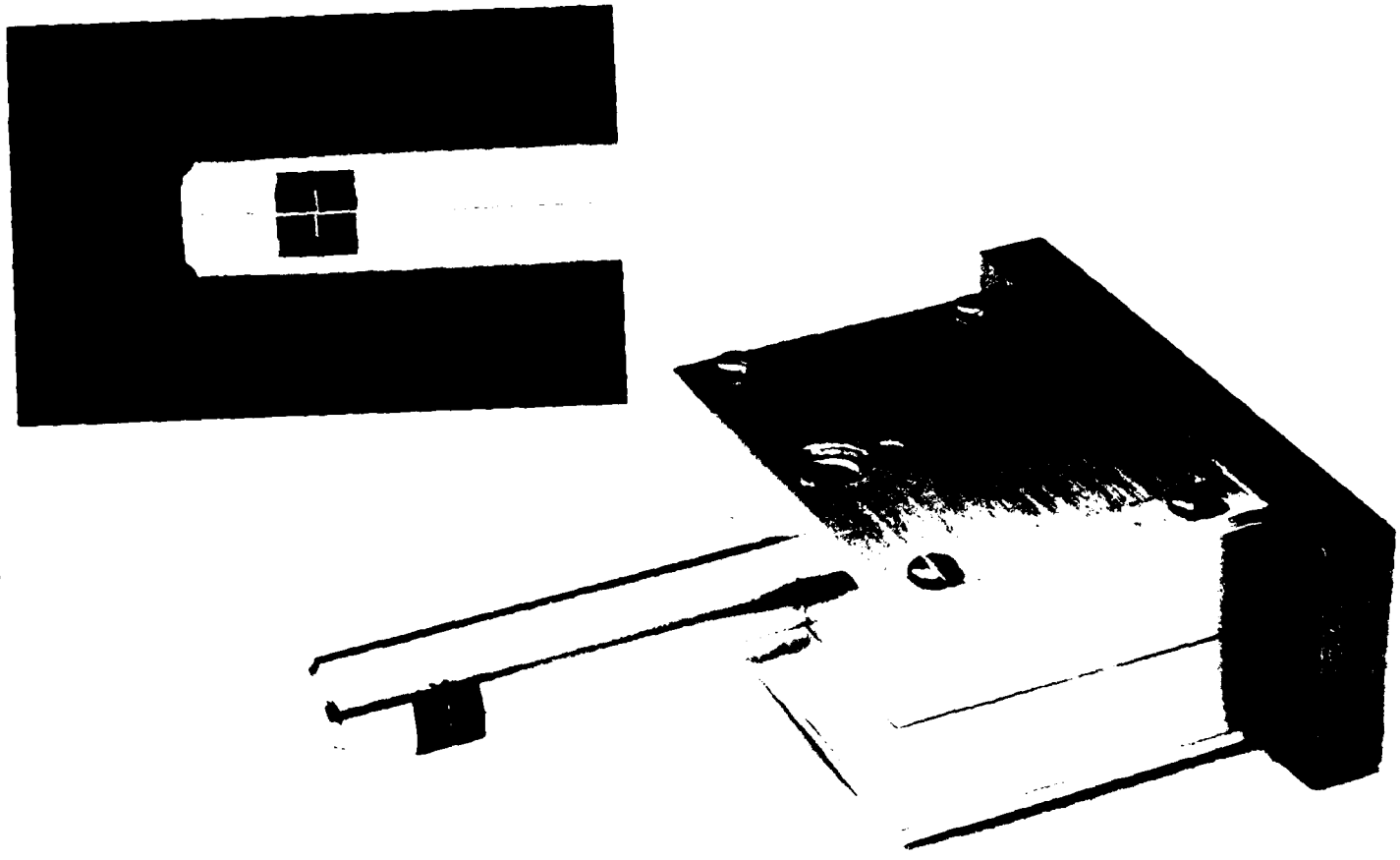

(b) ASSEMBLED

FIGURE 15 (CONCLUDED)

absolute probe assembly (without the insulating tape) is shown in Figure 16. The defect sensitivity of this probe was 0.2 V, or about 18 dB less than that of the microwave probe.

3. Floppy-Disk Probe

The second floppy-disk head was ground so that its face conformed to the inside diameter of the hole in the sample and was mounted in a handle to facilitate manual scanning. Since the probe face was nonconductive, it could be placed in direct contact with the sample surface. A photograph of this absolute probe assembly is shown in Figure 17. Its measured defect sensitivity was only 0.03 V, or about 34 dB less that that of the microwave probe.

E. Probe Reproducibility and Temperature Sensitivity

1. Printed-Coil Probe

Four additional printed-coil probes were fabricated, thereby providing a total of five absolute probes with which the EDM slot in the annular ring could be scanned. The purpose of the data obtained in this way was to establish the degree to which replicas of this type of probe could consistantly characterize the shallow flaw. Each of the five probes was used to scan the flaw on three different days in order to provide a measure of the consistancy of the data for each probe, as well as to determine the reproducibility of the data obtained with different probes.

Although the phenolic body of the probe was split by a sawcut along its axis (see Figure 16) in an effort to provide a tight fit between the probe body and the hole, the contact pressure varied between the different probes because the body diameters varied by about ±0.002 in. The probes that fitted the hole tightly would bind while being scanned, and generated relatively large lift-off/background signals. On the other hand, the probes that fitted the hole loosely required the use of great care during scanning to prevent excessive lift-off variations.

FIGURE 16 PRINTED-COIL HOLE-INSPECTION PROBE

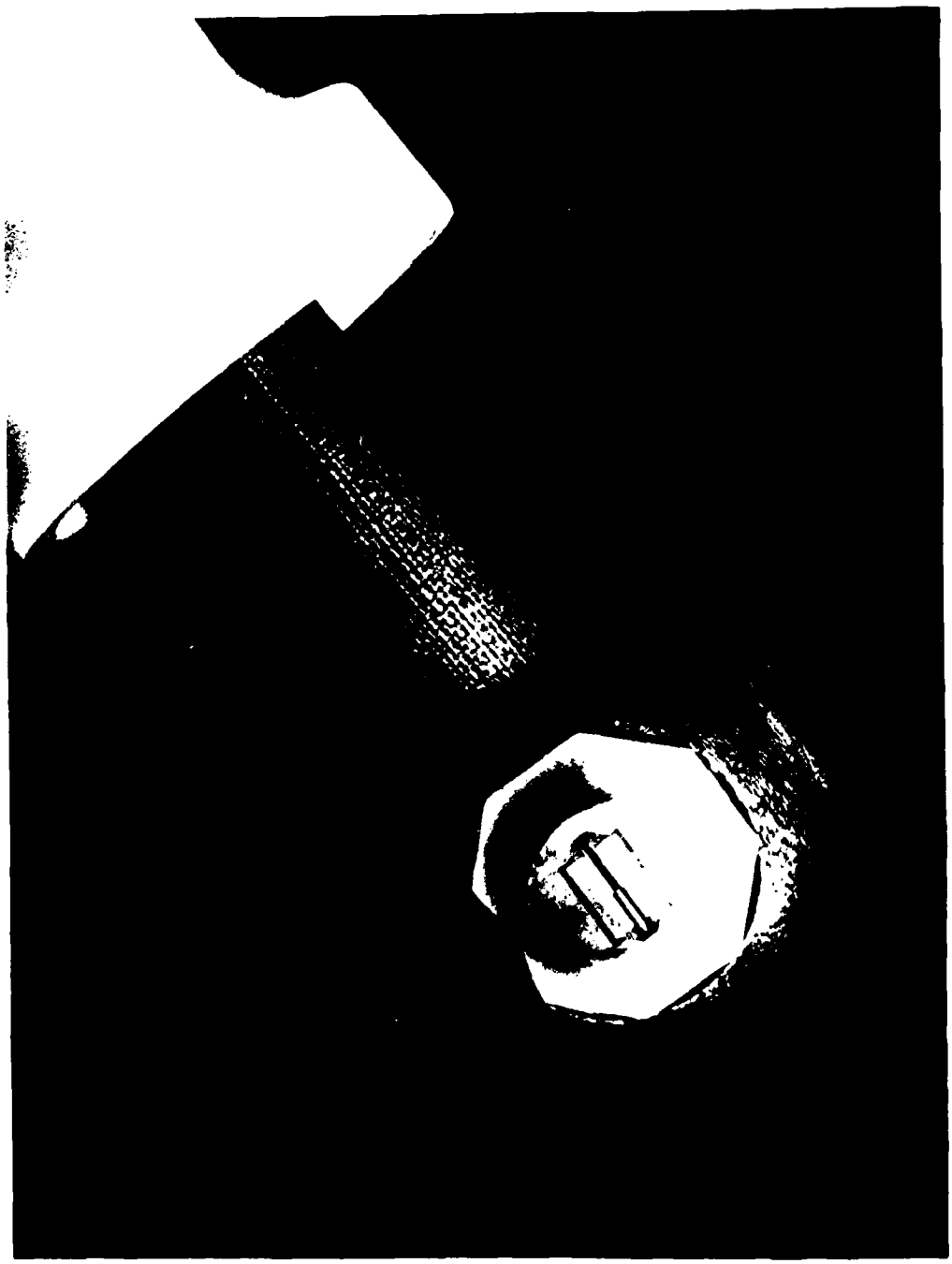

FIGURE 17 FLOPPY-DISK HOLE-INSPECTION PROBE

A summary of the measured defect sensitivities for the three sets of data is given in Table 1. The probes that exhibited the highest defect sensitivities (1 and 4) were those that fit most tightly in the hole, while the lower sensitivities were obtained with the looser-fitting probes. We therefore concluded that lift-off is a major factor in determining the flaw-response reproducibility of this probe. The reproducibility of the printed coil itself was very good and was not a contributor to the observed variations in flaw response.

Table 1

MEASURED DEFECT SENSITIVITIES FOR PRINTED-COIL PROBES (volts)

Data Set	Probe Number				
	1	2	3	4	5
A	0.2	0.16	0.16	0.18	0.15
B	0.2	0.15	0.16	0.18	0.16
C	0.2	0.16	0.15	0.17	0.16

The variation in probe response with changes in temperature was also measured using printed-coil probe 2. The technique used was to place the annular sample (which had a relatively large thermal mass) on a hot plate and slowly raise the temperature to about 50°C. The probe was installed in the sample for the duration of the test, and therefore the temperature of the printed-coil probe also was raised. The RF-bridge isolation changed less than 3 dB and was greater than 26 dB for the duration of the test. The system null was maintained by readjusting the null box before each measurement. Data were taken at 24°C, 46°C, 50°C, and 53°C, both as the sample warmed up and again as it cooled. The defect sensitivity of the probe remained essentially constant during these heating and cooling cycles. However, the probe showed an increase in sensitivity of about 10 percent after being at 53°C for a while, and it exhibited this improved

sensitivity until it was completely cool again. It was noticed that the probe became noticeably tighter in the hole at the elevated temperature, and so we conclude that the observed sensitivity variation was due to a change in lift-off, possibly caused by temperature-related dimensional changes in the Scotch tape that was used to insulate the probe from the sample.

2. Microwave Probe

In an effort to minimize possible manufacturing differences between probes, the matching network in the microwave probe was redesigned using an etched spiral inductor in place of the hand-wound inductor used in earlier realizations. In addition, a trimming capacitor was incorporated to facilitate resonator matching. With these changes in the matching network, 50 dB of RF-bridge isolation could be obtained when the probe and sample were aligned carefully.

To evaluate the probe's reproducibility, two sets of printed circuit boards were fabricated. The first set was assembled in the probe body, and this probe was used to scan the titanium annular ring. A symmetrical differential response was obtained, and a defect sensitivity of 3.3 V was measured. Without changing the alignment of the mechanical stage, the probe assembly was removed and the second set of circuit boards was installed. The probe assembly then was reinstalled on the bridge and the annular sample was scanned again. This probe's response was found to be unsymmetrical and exhibited a defect sensitivity of only 1.6 V. In an effort to explain this variation between the two probes, the probe dimensions were measured using a microscope. It was determined that the 0.010-in.-wide strip that short circuits the microstrip to the ground plane was recessed about 0.005 in. more in the poorer probe than the other; in addition, the short-circuiting strip in the poorer probe was shifted laterally nearly 0.002 in. This large difference in probe performance emphasizes the need for stringent mechanical tolerances in the fabrication of eddy-current probes intended to characterize small flaws. Small differences in probe-to-sample spacing produce relatively large differences in defect sensitivities.

F. Summary of Experimental Results

The performances of three different novel eddy-current-probe realizations operating at widely separated frequencies have been evaluated using both open and closed surface-connected flaws in metal samples. The defect sensitivity, defined as the amplitude of the signal produced by the defect under standardized test conditions, was used as the primary figure of merit in this probe comparison.

The measured defect sensitivities of all the different probes tested are shown in Table 2. These results can be summarized as follows:

- The microwave (1-GHz) probe achieved the greatest sensitivity to open slots. However, it was also very sensitive to lift-off and required that stringent mechanical tolerances be maintained during fabrication to achieve reproducibility.
- The floppy-disk (100-kHz) probe achieved the greatest sensitivity to closed cracks. However, it was not very sensitive to the small EDM slot in the titanium annulus, possibly because of difficulties in making the probe surface conform to the curved surface of the hole.
- The printed-coil (125-MHz) probe operated at a frequency intermediate to the frequencies used for the microwave and floppy-disk probes, and, interestingly enough, exhibited intermediate levels of defect sensitivity, as well as an intermediate sensitivity to lift-off.

These results suggest, in general, that high frequencies should be used to detect open cracks, and that lower frequencies should be used to detect closed cracks. However, it should be kept in mind that the observed differences in crack sensitivity also could be caused in part by differences in probe material and geometry.

Table 2

SUMMARY OF DEFECT SENSITIVITIES FOR
SEVERAL DIFFERENT EDDY-CURRENT PROBES

Probe	Aluminum Plate (Slot 3)	Titanium Plate (Slot C)	Titanium Annulus (EDM Slot)	Closed Fatigue Cracks	
				B-3	C-3
Absolute Coil (100 kHz)	2.2 V	0.04 V	---	0.5 V	1.0 V
Differential Coil (100 kHz)	1.4 V	0.08 V	---	1.5 V	2.4 V
Floppy-Disk Head (100 kHz)	6 V	0.8 V	0.03 V	6 V	6.4 V
Printed-Coil (125 MHz)	10 V	3.1 V	0.2 V	1.2 V	0.9 V
Microwave Probe 2 (1 GHz)	>15 V	9 V	1.6 V	0.7 V	0.3 V

IV SUMMARY AND CONCLUSIONS

An extensive circuit analysis of a generalized eddy-current system has been performed using an equivalent circuit. This analysis shows the relationship between probe and bridge impedances that is required for maximum sensitivity. Furthermore, the analysis shows that the sensitivity is proportional to the ratio of the change in probe impedance produced by a flaw to the unperturbed probe impedance.

The current status of the electromagnetic field analysis required to characterize the interaction between an eddy-current probe and a flaw has been reviewed. In its present form, the analysis predicts that a probe's sensitivity to open cracks can be increased by operating at microwave frequencies. In addition, the analysis shows that the sensitivity is strongly dependent on the magnetic field generated per unit of driving current, as well as the probe's ability to concentrate this field in the region of the flaw. These qualitative predictions have been verified by experiment. However, further development of the theory will be needed to improve its ability to make quantitative predictions. For example, such features of realistic eddy-current testing as nonuniform excitation and irregular flaw shapes will have to be taken into account.

The performances of three different novel eddy-current-probe realizations operating at widely separated frequencies have been evaluated using both open and closed surface-connected flaws in metal samples. These probes consisted of a 1-GHz microstrip-resonator probe, a 125-MHz printed-coil probe, and a 100-kHz modified floppy-disk head. All three of these probes were more sensitive to open slots than the commercial 100-kHz probes that were used as references, with the microwave probe being the most sensitive. On the other hand, only the floppy-disk head was more sensitive to closed cracks than the commercial probes. In general, these results suggest that high frequencies should be used to detect open cracks, and

lower frequencies should be used to detect closed cracks. However, it should be kept in mind that the observed differences in crack sensitivity also could be caused in part by differences in probe material and geometry.

In general, the high-frequency probes were also more sensitive to lift-off than the low-frequency probes. Again, this behavior can be attributed partly to differences in probe material and geometry, as well as to differences in frequency. In general, though, it appears that high-frequency eddy-current probes tend to exhibit higher lift-off sensitivity than do low-frequency probes.

It is difficult to draw any general conclusions concerning the ability of the various probes to discriminate between a signal produced by a variation in lift-off and one produced by a flaw. Lift-off discrimination not only depends on the phase between the signals, but also on their relative amplitudes. In other words, it is often possible to discern a relatively large flaw signal even when its phase is the same as the phase of the lift-off signal. Thus, the microwave probe was able to detect the small EDM slot in the titanium annular ring more readily than the other two probes, even though their responses to this slot were orthogonal to their lift-off responses.

The printed-circuit portions of the microwave probe and the printed-coil probe were very reproducible. In spite of this, some variations in the responses of different probes of the same type to a given flaw were observed. These were most likely due to variations in the probe-to-sample distance of the different probes, which were caused by construction differences between the probes that occurred when the printed circuits were mounted in a housing to form a complete probe. Hence, the use of printed circuits in an eddy-current probe does not in itself guarantee good response reproducibility.

Thus, to obtain the same flaw response with different probes of the same type and operating frequency, it is necessary that all portions of the eddy-current system be replicated with suitable precision.* The

---

*The degree of precision required must be determined for each type of probe and/or measurement system.

parts of the system that need particular attention in this regard are (1) the sensor (particularly the lift-off distance and the probe dimensions) and, (2) the impedance-matching network.

In summary, we have shown that a microwave-frequency microstrip resonator used as an eddy-current probe is significantly more sensitive to open surface-breaking flaws than a conventional eddy-current probe. However, the construction of a microwave probe is more complicated and expensive, and the control of lift-off distance is more critical.

On the other hand, the printed-coil probe is fairly simple and inexpensive to construct. It also offers very good sensitivity to open flaws, and its sensitivity to closed flaws is comparable to that of conventional probes. Moreover, this probe is not rigid like the microwave probe, and therefore can be moved by hand. However, the printed-coil probe must operate in the tens-of-MHz range to achieve a resonable impedance level (unless some kind of impedance transformer is used), and so, like the microwave probe, it requires the use of frequency conversion, which in turn slightly complicates the eddy-current system.

A modified floppy-disk head has been found to function very well as an eddy-current probe. Its sensitivity to both the open and closed reference flaws was at least 10 dB higher than that of conventional probes operating at the same frequency. This type of probe uses a low-reluctance ferrite yoke to guide and shape the magnetic field generated by a driving coil, and is nonresonant, both electromagnetically and ferromagnetically. In addition, the ability of this probe's ferrite yoke to guide and shape the magnetic field suggests several interesting possibilities, such as designing a probe to inspect the corners of bolt holes. We recommend that additional work be performed to evaluate and develop this type of probe.

In conclusion, the microwave probe developed during this program seems very well suited for detecting small open flaws in parts that can be mechanically scanned past a fixed probe. The printed-coil intermediate-frequency probe offers good sensitivity to both open and closed flaws, good reproducibility, and moderate maneuverability. Therefore, for the proper application, both of these probes should provide an improved capability in eddy-current testing.

Appendix

MEASURED PERFORMANCE OF EDDY-CURRENT INSPECTION PROBES

Appendix

MEASURED PERFORMANCE OF EDDY-CURRENT INSPECTION PROBES

A. Description of Flawed Test Samples

Several flat-plate samples with surface-connected flaws were available for inspection. Four such samples were chosen for use in the probe evaluation.

Two of the plates had shallow electrodischarge-machined (EDM) slots. One plate was aluminum and contained six EDM slots, which were also of different sizes. Silicon rubber replicas of the slots in the aluminum sample had been made previously and examined with a scanning electron microscope (SEM). SEM photographs of these replicas showing their dimensions are shown in Figure A-1. The slots in the titanium sample were photographed and measured using an optical microscope. Photographs showing these slots and their surface dimensions are shown in Figure A-2.

The remaining two flat-plate samples contained fatigue cracks. Both samples were 2024-T3 aluminum, and each contained a single closed crack. A photograph of the one of these cracks (sample B-3) is shown in Figure A-3. Its length is 0.182 in. The crack in the other sample (C-3) was very similar in appearance, but more tightly closed and therefore more difficult to photograph. The length of the crack in this sample was 0.252 in.

The one non-planar sample used in this probe evaluation was a titanium split annular ring having a 1-in.-diameter hole. There was a shallow EDM slot on the inner surface of the hole. Its dimensions were measured under a microscope and were found to be:

Length: 338 μm (0.0133 in.)
Width: 156 μm (0.0061 in.)
Depth: 40 μm (0.0016 in.)

19X 100X

(a) SLOT 1: WIDTH = 0.010 in., LENGTH = 0.100 in., DEPTH = 0.010 in.

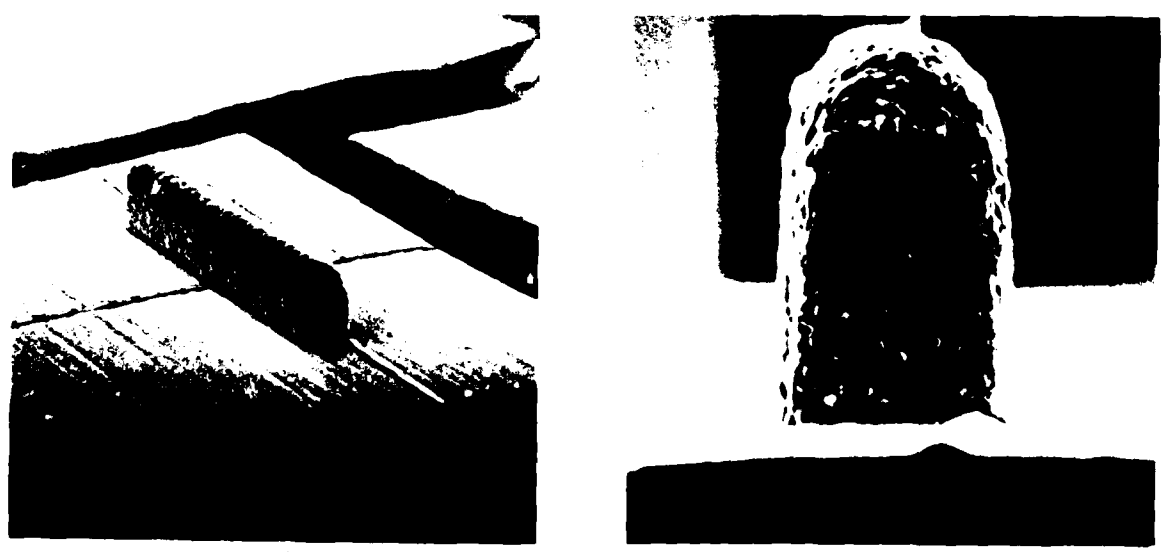

20X 100X

(b) SLOT 2: WIDTH = 0.010 in., LENGTH = 0.100 in., DEPTH = 0.021 in.

FIGURE A-1 REPLICAS OF EDM SLOTS IN ALUMINUM CALIBRATION PLATE

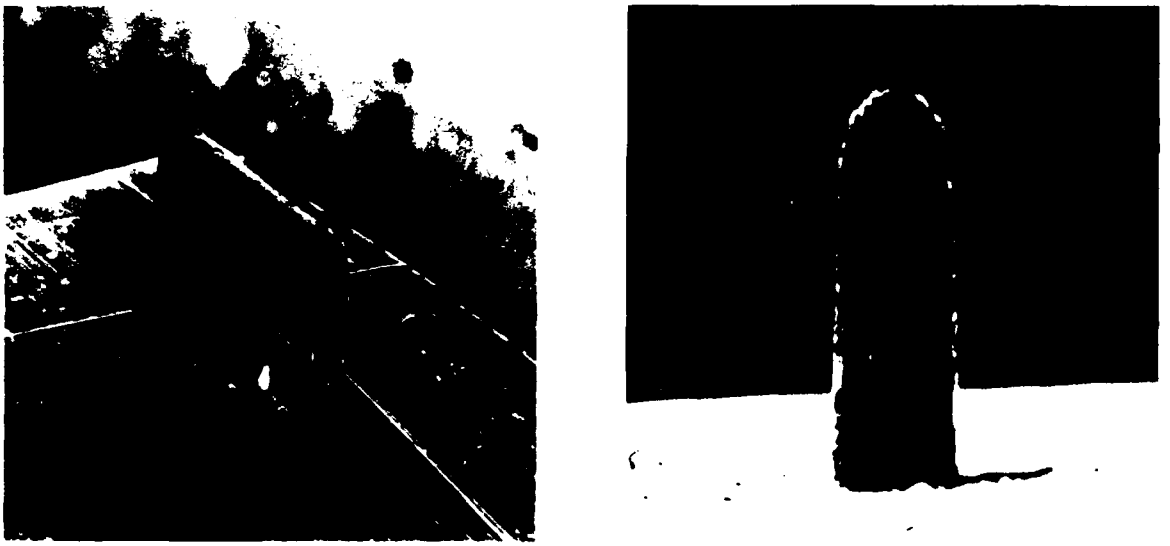

18X 50X

(c) SLOT 3: WIDTH = 0.010 in., LENGTH = 0.100 in., DEPTH = 0.044 in.

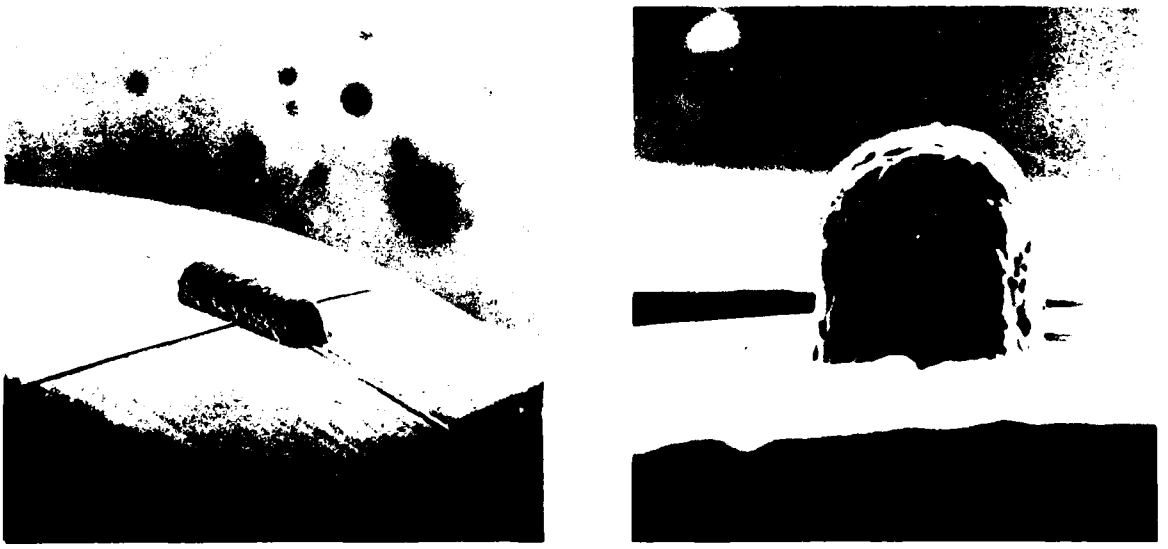

20X 100X

(d) SLOT 4: WIDTH = 0.010 in., LENGTH = 0.050 in., DEPTH = 0.013 in.

FIGURE A-1 (Continued)

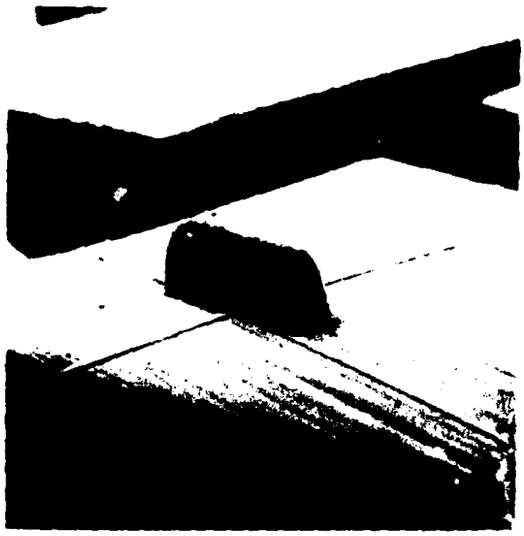

20X

100X

(e) SLOT 5: WIDTH = 0.010 in., LENGTH = 0.050 in., DEPTH = 0.023 in.

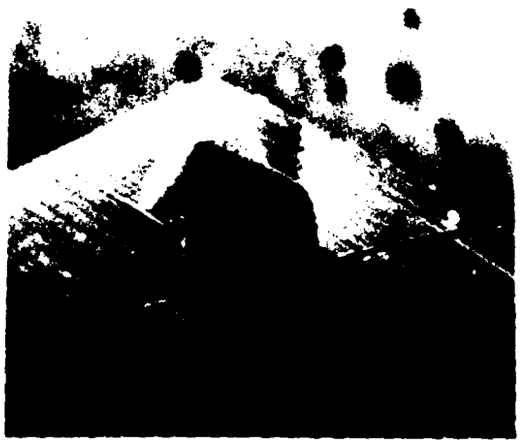

20X

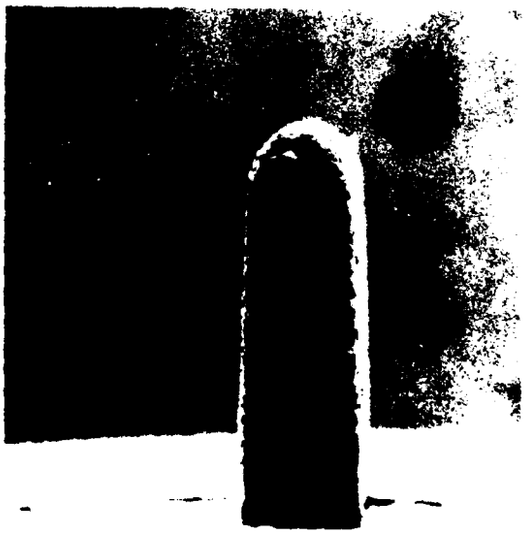

50X

(f) SLOT 6: WIDTH = 0.010 in., LENGTH = 0.050 in., DEPTH = 0.046 in.

FIGURE A-1 (Concluded)

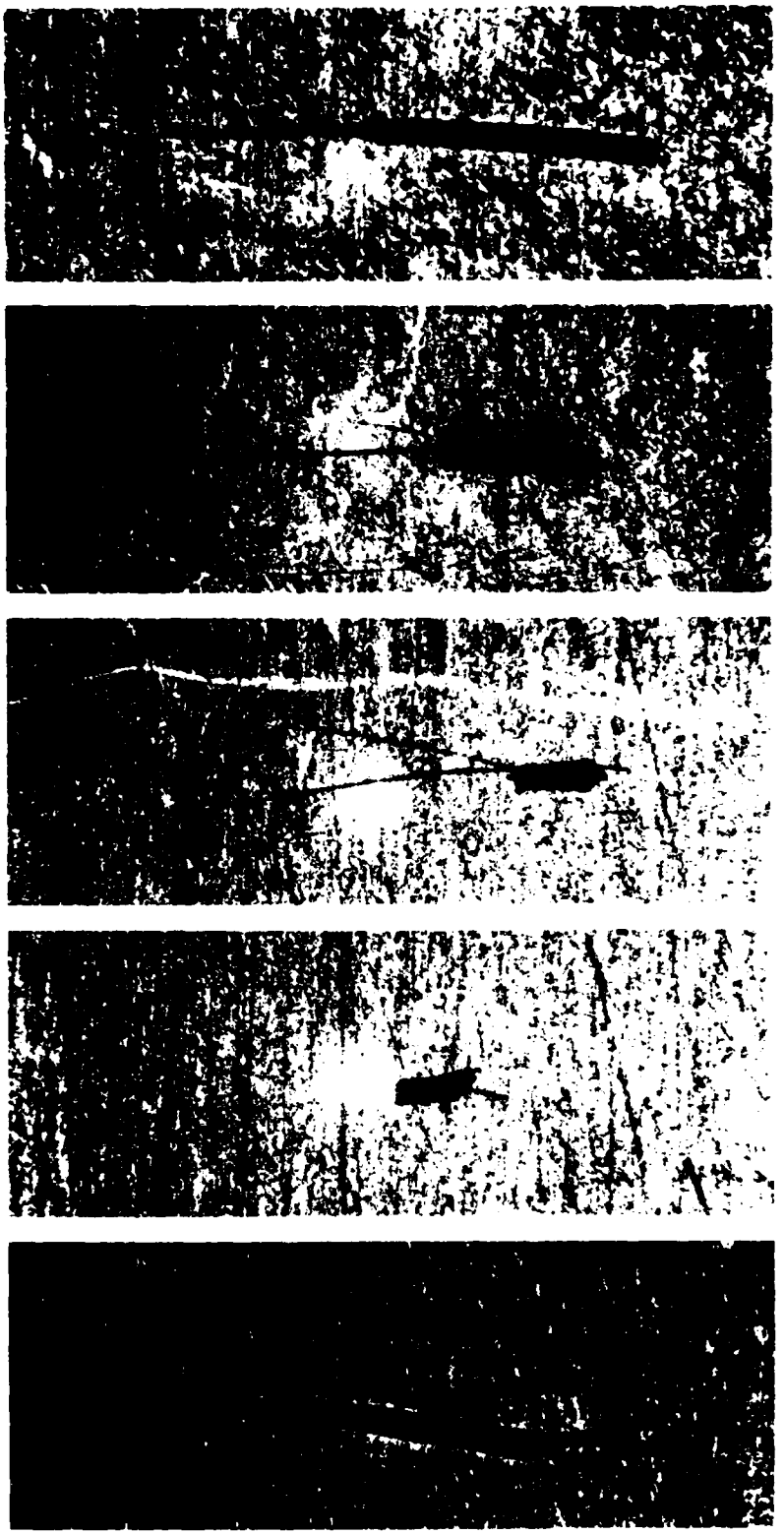

(a) SLOT A: WIDTH = 0.010 in.
LENGTH = 0.113 in.

(b) SLOT B: WIDTH = 0.010 in.
LENGTH = 0.060 in.

(c) SLOT C: WIDTH = 0.010 in.
LENGTH = 0.033 in.

(d) SLOT D: WIDTH = 0.010 in.
LENGTH = 0.029 in.

(e) SLOT E: WIDTH = 0.010 in.
LENGTH = 0.103 in.

FIGURE A-2 EDM SLOTS IN TITANIUM PLATE (15X)

SAMPLE B-3
CRACK LENGTH = 0.182 in.

FIGURE A-3 FATIGUE CRACK IN 2024-T3 ALUMINUM SAMPLE (500X)

The major axis of this slot was aligned with the axis of the hole, and the slot was positioned halfway down the 1-in.-long hole. A photograph of this slot is shown in Figure A-4.

B. Individual Probe Responses

The measurement system was calibrated, as discussed in Section III-B, so that the defect sensitivity for each probe could be read directly from the phasor display on the storage oscilloscope. The defect sensitivity was defined here as the magnitude of the phasor flaw response. Nortec probes (Models SP-100, SP/DP-100, and DP-64) were used as references by which the various experimental probes' performances could be compared. The performance of each probe is described in the following sections.

1. Nortec Model SP-100

The responses of this commercial absolute probe at 100 kHz to representative flaws in flat plates are shown in Figures A-5 and A-6. This

FIGURE A-4 EDM SLOT IN TITANIUM ANNULAR RING

probe could easily detect large open slots such as slot 3 in the aluminum calibration plate (Figure A-5[a]). However, small open slots such as slot C in the titanium sample were barely discernable (Figure A-5[b]). The lift-off discrimination for small open slots was also poor.

The closed cracks in samples B-3 and C-3 could be detected easily (Figure A-6), although the signal amplitude was 10 to 16 dB less than that produced by the large open slot in the aluminum calibration plate (slot 3). The lift-off discrimination for both of the closed cracks that were tested was acceptable.

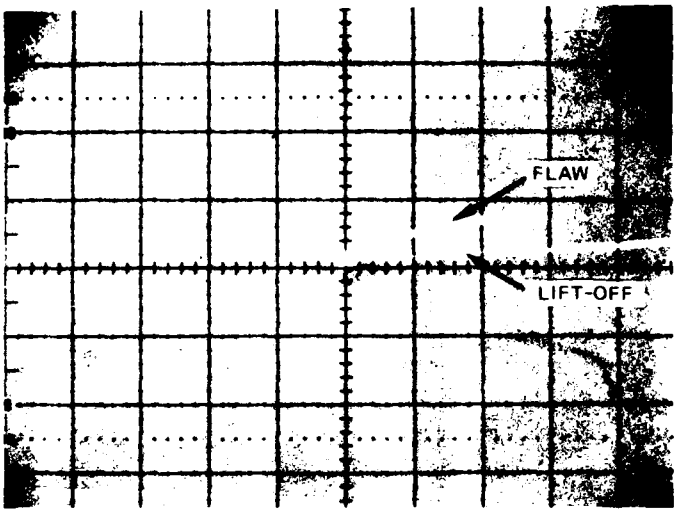

(a) ALUMINUM CALIBRATION PLATE, SLOT 3

DISPLAY SENSITIVITY = 1 V/div (both axes)

DEFECT SENSITIVITY ~ 2.2 V

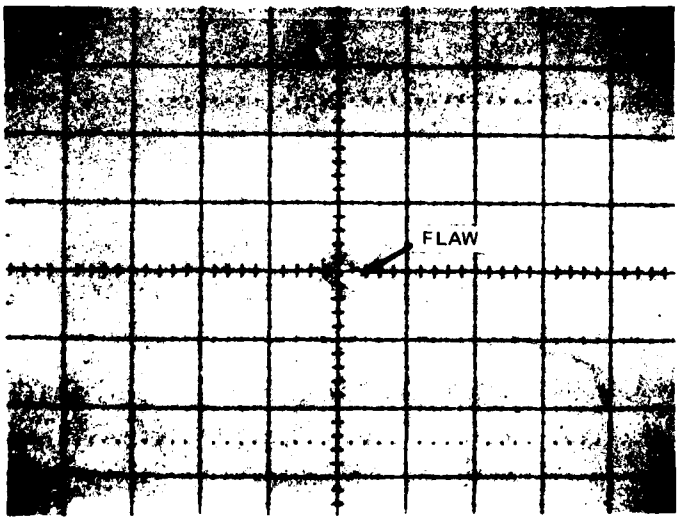

(b) TITANIUM PLATE, SLOT C

DISPLAY SENSITIVITY = 0.1 V/div (both axes)

DEFECT SENSITIVITY ~ 0.04 V

NOTE: The lift-off response is not shown here because it is in the same direction as the flaw response and tends to obscure it.

FIGURE A-5 RESPONSES OF NORTEC PROBE (Model SP-100) TO SHALLOW EDM SLOTS

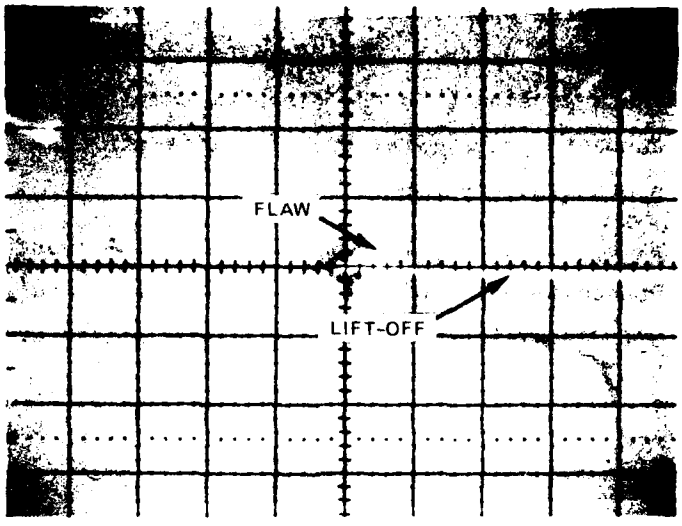

(a) 2024-T3 ALUMINUM, SAMPLE B-3

DISPLAY SENSITIVITY = 0.5 V/div (both axes)

DEFECT SENSITIVITY ~ 0.5 V

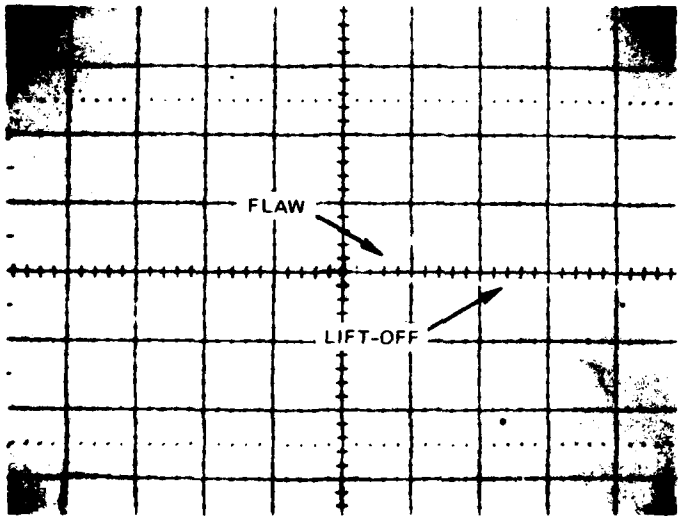

(b) 2024-T3 ALUMINUM, SAMPLE C-3

DISPLAY SENSITIVITY = 0.5 V/div (both axes)

DEFECT SENSITIVITY ~ 1.0 V

FIGURE A-6 RESPONSES OF NORTEC PROBE (Model SP-100) TO CLOSED FATIGUE CRACKS

2. Nortec Model SP/DP-100

The responses of this commercial differential probe at 100 kHz to the same flaws in flat plates are shown in Figures A-7 and A-8. This probe can also easily detect large open slots (such as slot 3) in the aluminum calibration plate (Figure A-7[a]). The sensitivity of this probe to small open slots such as slot C in the titanium sample was greater than that of the absolute probe (SP-100). The lift-off discrimination for the open slots was very good.

The sensitivity to the closed cracks in samples B-3 and C-3 was equal to or better than the sensitivity to slot 3 in the aluminum calibration plate. The lift-off discrimination for both of the closed cracks was very good.

3. Nortec Model DP-64

This probe is a 100-kHz differential probe made specifically for inspecting 1-in.-diameter holes. It was used only to scan the titanium annular ring. For the signal levels used, the shallow EDM slot in the annular ring was not detectable using this probe.

4. Microwave Probe 1

The initial probe design (shown schematically in Figures 10 and A-9[a]) was able to detect relatively large open slots at 1 GHz, as is shown by the responses in Figure A-10; however, smaller slots such as slot C in the titanium sample could not be detected. This probe also was unable to detect the fatigue cracks in aluminum samples B-3 and C-3. It was concluded that the sensitivity could be improved by narrowing the probe tip to increase the magnetic field at the netal surface.

5. Microwave Probe 2

This 1-GHz probe is shown schematically in Figure A-9(b), and was designed to increase the magnetic field at the resonator tip by decreasing the width of the circuit at that point. In order to minimize the effects of electric fringing fields, the circuit was tapered to a width of about 0.010 in. near the tip. This probe exhibited significantly

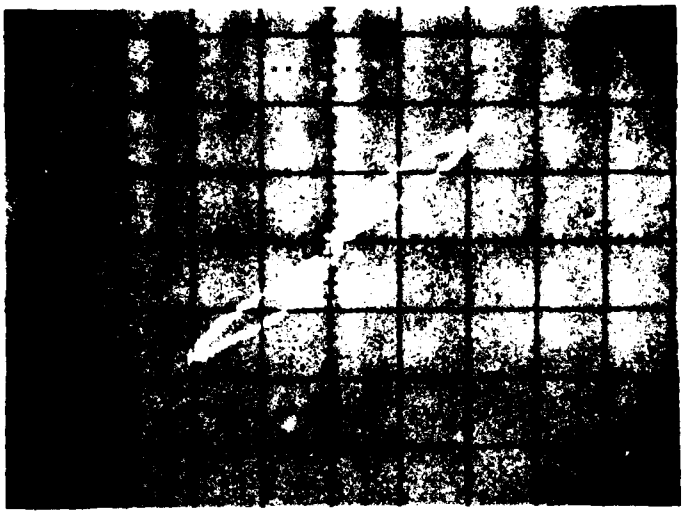

(a) **ALUMINUM CALIBRATION PLATE, SLOT 3**

DISPLAY SENSITIVITY = 0.5 V/div (both axes)

DEFECT SENSITIVITY ~ 1.4 V

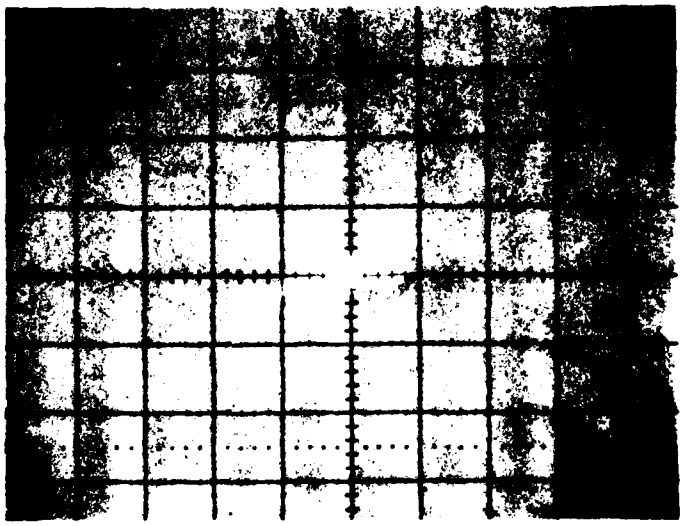

(b) ***TITANIUM PLATE,*** **SLOT C**

DISPLAY SENSITIVITY = 0.1 V/div (both axes)

DEFECT SENSITIVITY ~ 0.08 V

FIGURE A-7 RESPONSES OF NORTEC PROBE (Model SP/DP-100) TO SHALLOW EDM SLOTS

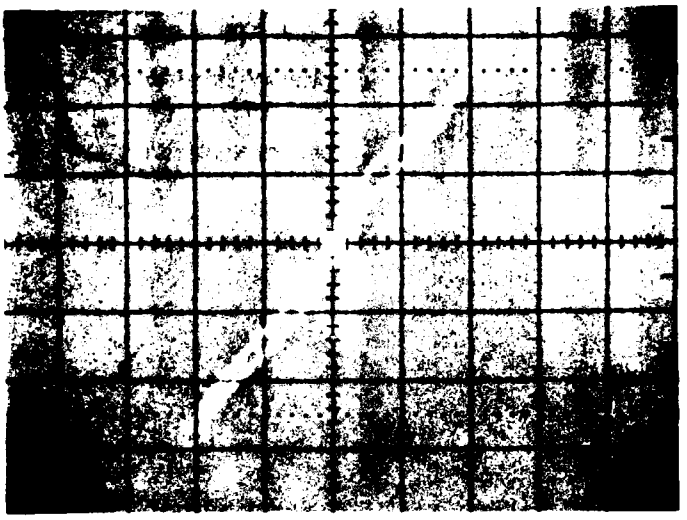

(a) 2024-T3 ALUMINUM, SAMPLE B-3

DISPLAY SENSITIVITY = 0.5 V/div (both axes)

DEFECT SENSITIVITY ~ 1.5 V

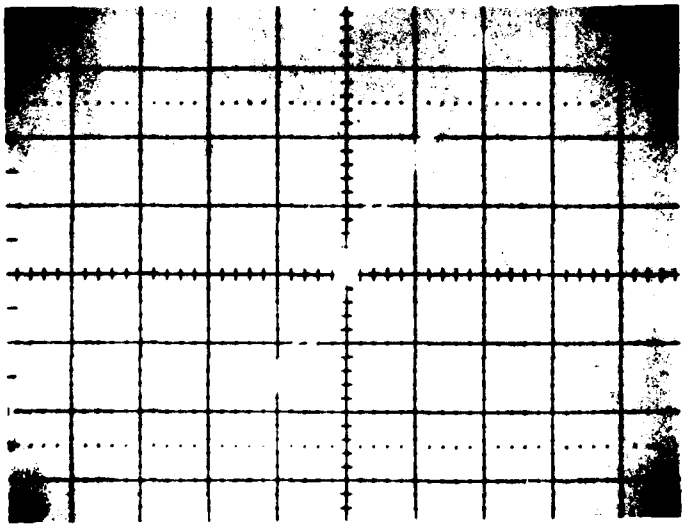

(b) 2024-T3 ALUMINUM, SAMPLE C-3

DISPLAY SENSITIVITY = 1.0 V/div (both axes)

DEFECT SENSITIVITY ~ 2.4 V

FIGURE A-8 RESPONSES OF NORTEC PROBE (MODEL SP/DP-100) TO CLOSED FATIGUE CRACKS

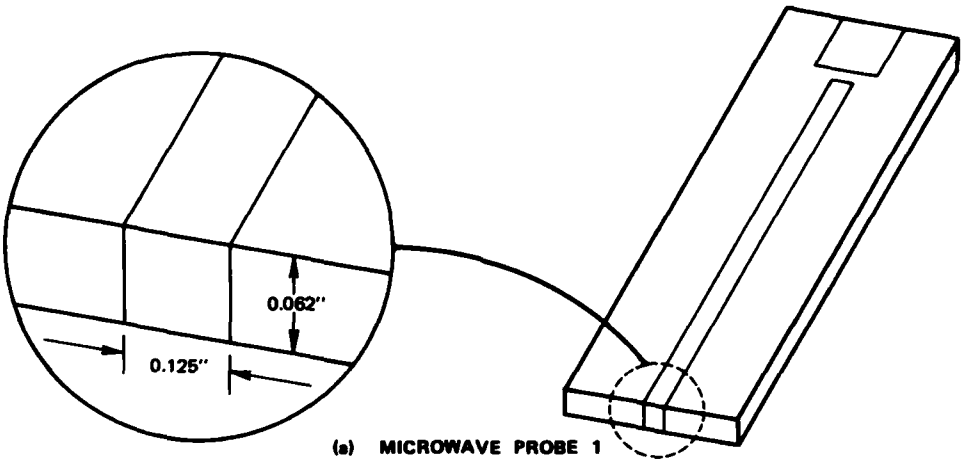

(a) MICROWAVE PROBE 1

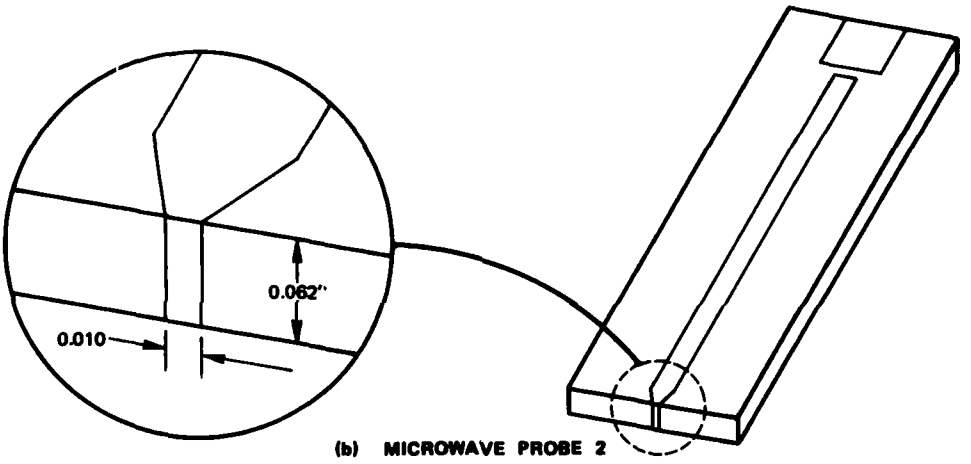

(b) MICROWAVE PROBE 2

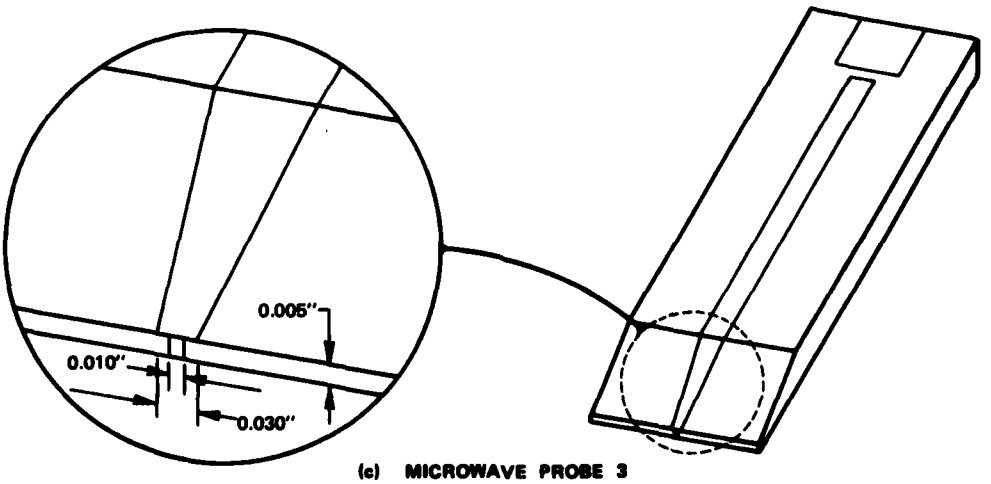

(c) MICROWAVE PROBE 3

FIGURE A-9 SCHEMATIC ILLUSTRATION OF THREE MICROWAVE PROBE DESIGNS

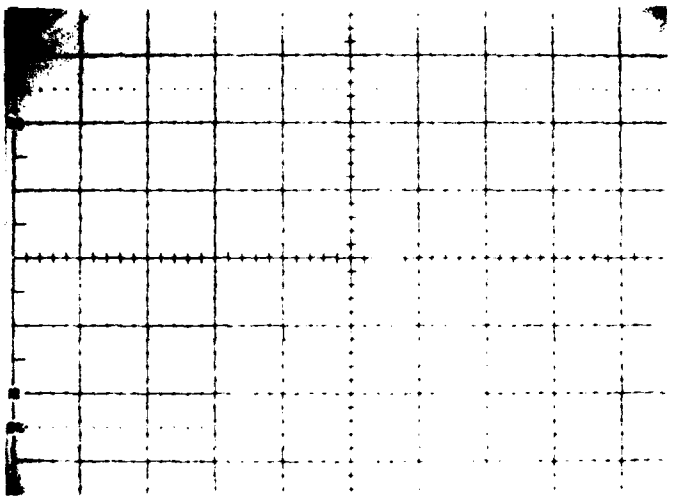

(a) ALUMINUM CALIBRATION PLATE, SLOT 3

DISPLAY SENSITIVITY = 0.5 V/div (both axes)

DEFECT SENSITIVITY ~ 0.8 V (both probes)

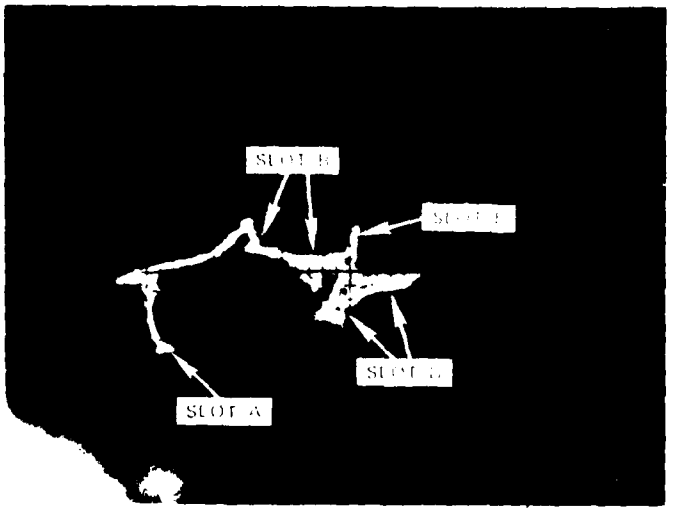

(b) TITANIUM PLATE, ALL 5 SLOTS (slot C could not be detected)

DISPLAY SENSITIVITY = 0.5 V/div (both axes)

FIGURE A-10. RESPONSES OF MICROWAVE PROBE 1 TO SHALLOW EDM SLOTS

better sensitivity in comparison with probe 1. In fact, the larger slots now saturated the measurement system, as can be seen in Figure A-11(a). Figure A-11(b) indicates that probe 2 had about 45 dB greater sensitivity to slot C in the titanium sample than the commercial probe. In addition, the lift-off discrimination of probe 2 was excellent.

The sensitivity of probe 2 to closed cracks, however, did not improve as expected. Although this probe could detect the closed cracks in both aluminum samples (see Figure A-12), its sensitivity was about equal to or less than that of the commercial probe.

6. Microwave Probe 3

In this design (shown in Figure A-9[c]) we attempted to increase the probe's sensitivity to electric field variations. The substrate was tapered to a 0.005-in.-thick edge. The circuit width also was tapered from 0.062 in. to 0.030 in. to minimize the impedance variation. The probe tip was formed by connecting a 0.10-in.-wide metal strip between the center-line of the 0.030-in.-wide microstrip and the ground plane. Since the microstrip was three times wider than the connecting strip, the electric fringing fields across the 0.005-in. gap should have been enhanced near the edges of the microstrip.

This probe was found to have less sensitivity than probe 2. Its sensitivity to open slots was about one-third that of probe 2, and its sensitivity to closed cracks was reduced by a factor of two. These data suggest that probes 2 and 3 have different relative sensitivities to slots and closed cracks. However, the control of probe-to-sample spacing during the recording of these data was not as precise as during later measurements; hence, differences in this spacing also could account for the observed relative differences in sensitivity.

Photographs illustrating the performance of probe 3 at 1 GHz are shown in Figures A-13 and A-14.

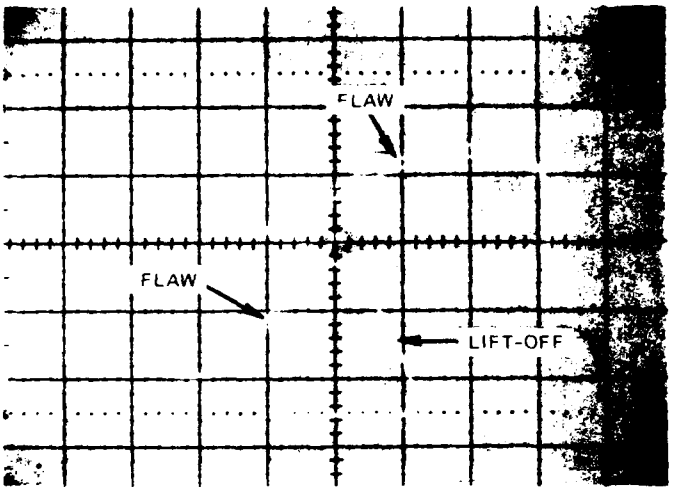

(a) ALUMINUM CALIBRATION PLATE, SLOT 3

DISPLAY SENSITIVITY = 5 V/div (both axes)

DEFECT SENSITIVITY IS GREATER THAN 15 V (system saturates for output signals near 15 V)

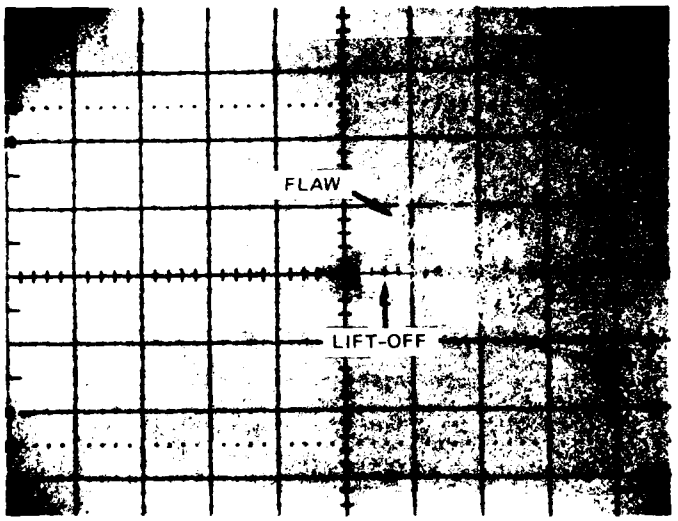

(b) TITANIUM PLATE, SLOT C

DISPLAY SENSITIVITY = 5 V/div (both axes)

DEFECT SENSITIVITY ~ 9 V

FIGURE A-11 RESPONSES OF MICROWAVE PROBE 2 TO SHALLOW EDM SLOTS

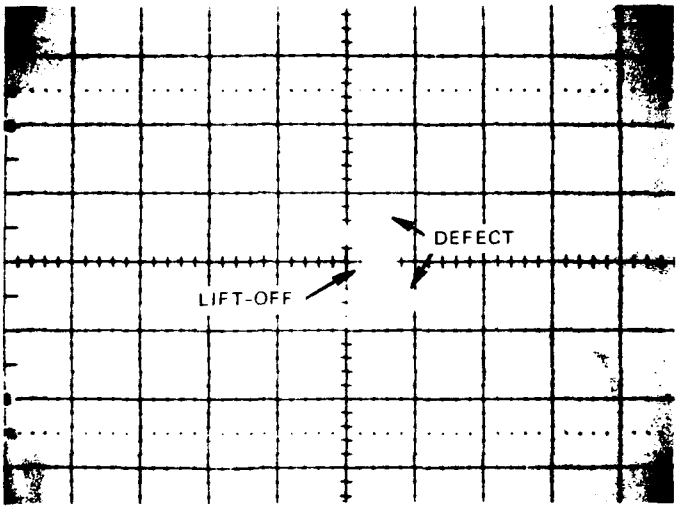

(a) 2024-T3 ALUMINUM, SAMPLE B-3

DISPLAY SENSITIVITY = 0.5 V/div (both axes)

DEFECT SENSITIVITY ~ 0.7 V

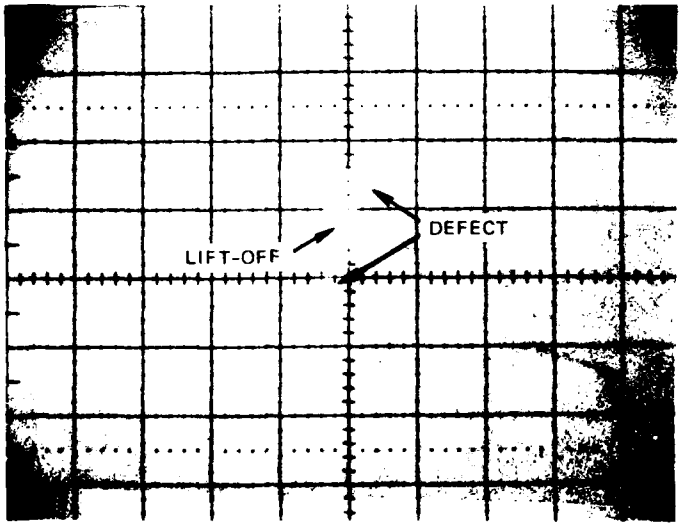

(b) 2024-T3 ALUMINUM, SAMPLE C-3

DISPLAY SENSITIVITY = 0.5 V/div (both axes)

DEFECT SENSITIVITY ~ 0.3 V

FIGURE A-12 RESPONSES OF MICROWAVE PROBE 2 TO CLOSED FATIGUE CRACKS

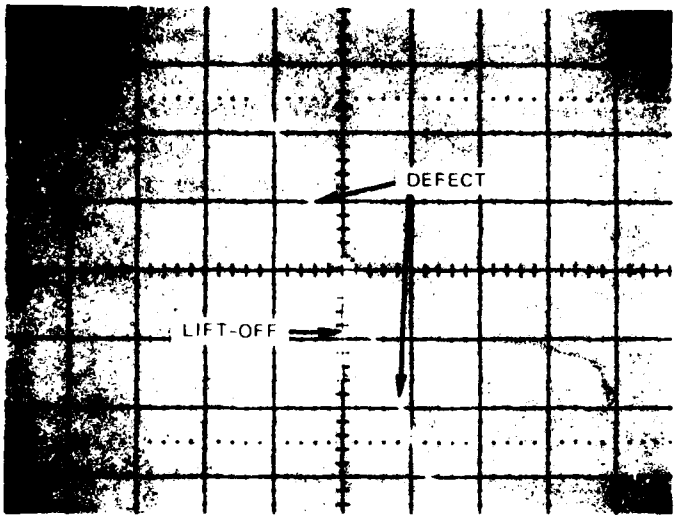

(a) ALUMINUM CALIBRATION PLATE, SLOT 3

DISPLAY SENSITIVITY = 2 V/div (both axes)

DEFECT SENSITIVITY ~ 6.5 V

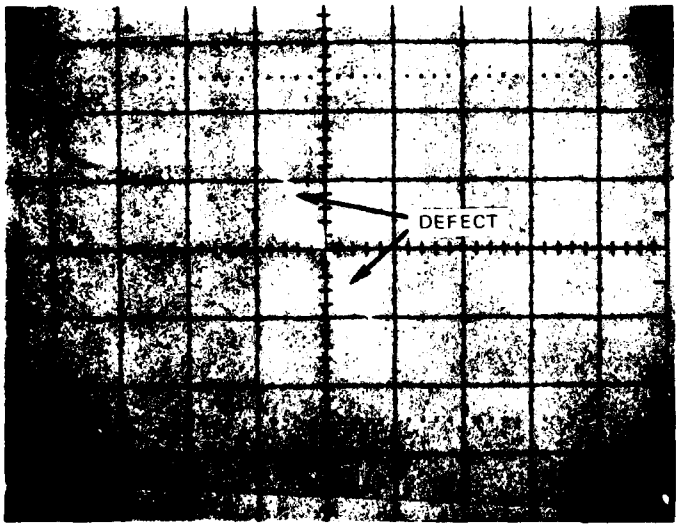

(b) TITANIUM PLATE, SLOT C

DISPLAY SENSITIVITY = 2 V/div (both axes)

DEFECT SENSITIVITY ~ 3 V

FIGURE A-13 RESPONSES OF MICROWAVE PROBE 3 TO SHALLOW EDM SLOTS

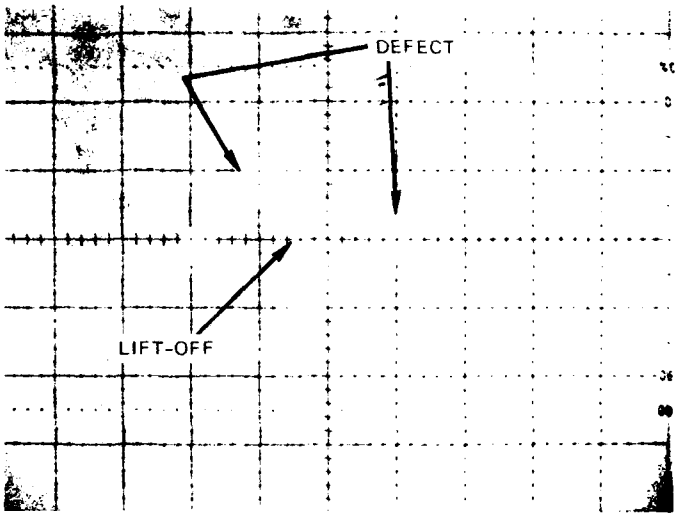

(a) 2024-T3 ALUMINUM, SAMPLE B-3

DISPLAY SENSITIVITY = 0.1 V/div (both axes)

DEFECT SENSITIVITY ~ 0.3 V

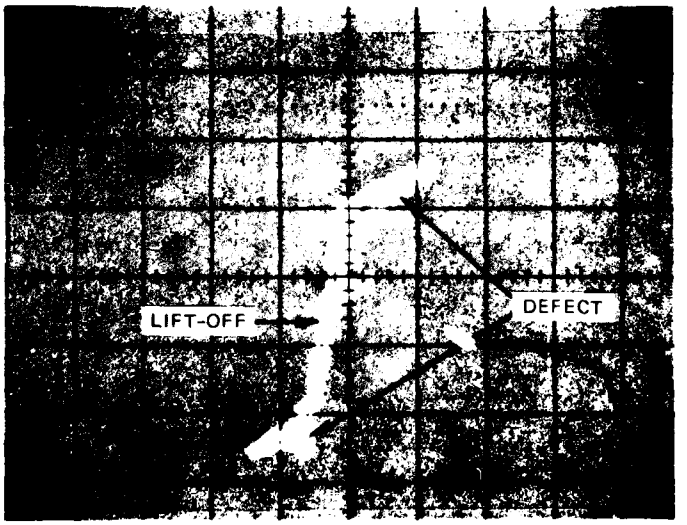

(b) 2024-T3 ALUMINUM, SAMPLE C-3

DISPLAY SENSITIVITY = 0.1 V/div (both axes)

DEFECT SENSITIVITY ~ 0.1 V

FIGURE A-14 RESPONSES OF MICROWAVE PROBE 3 TO CLOSED FATIGUE CRACKS

7. Printed-Coil Probe

This probe design consisted of an etched spiral inductor on a low-loss dielectric substrate (Duroid 5880), mounted at the end of a length of 50-Ω semi-rigid cable. The six-turn spiral had an outside diameter of about 0.1 in. and an inductance of approximately 30 nH. A photograph of this probe is shown in Figure 13.

The measured responses at 125 MHz of this absolute probe to the representative flaws in flat plates are shown in Figures A-15 and A-16. This probe is much more sensitive to the shallow EDM slots than the commercial absolute probe (SP-100), but its lift-off discrimination for the slots is poorer.

However, the sensitivity and lift-off discrimination of the printed-coil probe to closed cracks is comparable to the commercial probe.

8. Floppy-Disk Probe

In order to ascertain the utility of using a ferrite to concentrate and guide the magnetic field produced by a probe, two ferrite floppy-disk recording heads (Nortronics p/n H803019, button only) were evaluated as eddy-current probes at 100 kHz. As purchased, these heads had a spherical surface contour and a glass protective coating. One head was ground flat to provide a probe surface suitable for scanning the reference flaws in the flat plates. The other head was ground to conform to the inside diameter of the titanium annular ring and was used as a hole probe.

The measured 100-kHz responses of this absolute probe to the representative flaws in flat plates are shown in Figures A-17 and A-18. This probe's sensitivity to shallow EDM slots is much greater than that of the commercial absolute probe (SP-100). It has good lift-off discrimination for large slots (Figure A-17[a]) but poor lift-off discrimination for small slots (Figure A-17[b]).

This probe is also much more sensitive to the closed cracks than the commercial probe (Figure 18). Lift-off discrimination for both closed cracks was also very good.

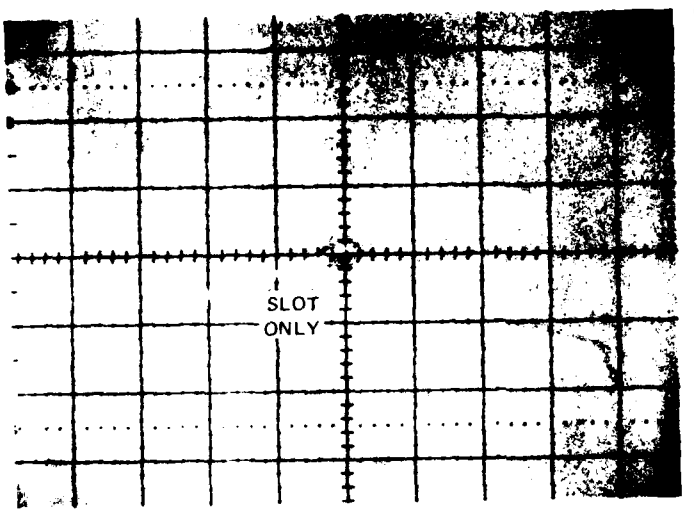

(a) ALUMINUM CALIBRATION PLATE, SLOT 3

DISPLAY SENSITIVITY = 5 V/div (both axes)

DEFECT SENSITIVITY ~ 10 V

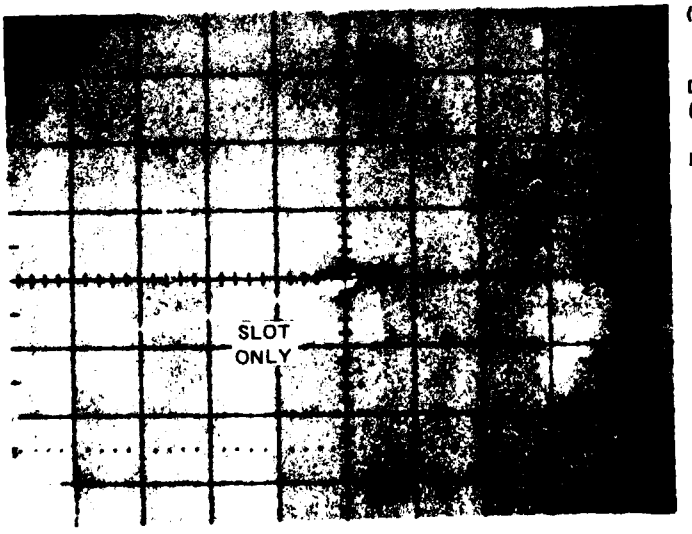

(b) TITANIUM PLATE, SLOT C

DISPLAY SENSITIVITY = 1 V/div (both axes)

DEFECT SENSITIVITY ~ 3.1 V

FIGURE A-15 RESPONSES OF PRINTED-COIL PROBE TO SHALLOW EDM SLOTS

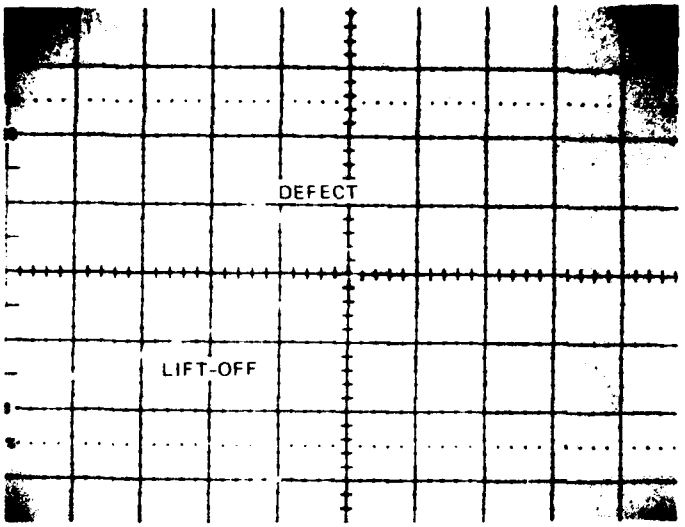

(a) 2024-T3 ALUMINUM, SAMPLE B-3

DISPLAY SENSITIVITY = 0.5 V/div (both axes)

DEFECT SENSITIVITY ~ 1.2 V

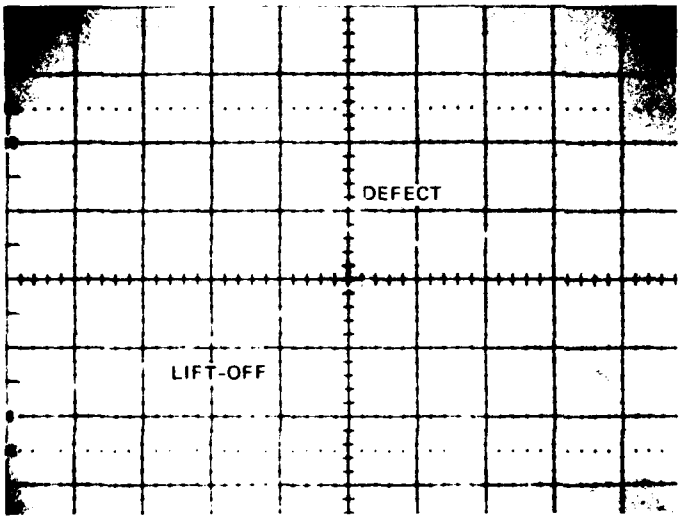

(b) 2024-T3 ALUMINUM, SAMPLE C-3

DISPLAY SENSITIVITY = 0.5 V/div (both axes)

DEFECT SENSITIVITY ~ 0.9 V

FIGURE A-16 RESPONSES OF PRINTED-COIL PROBE TO CLOSED FATIGUE CRACKS

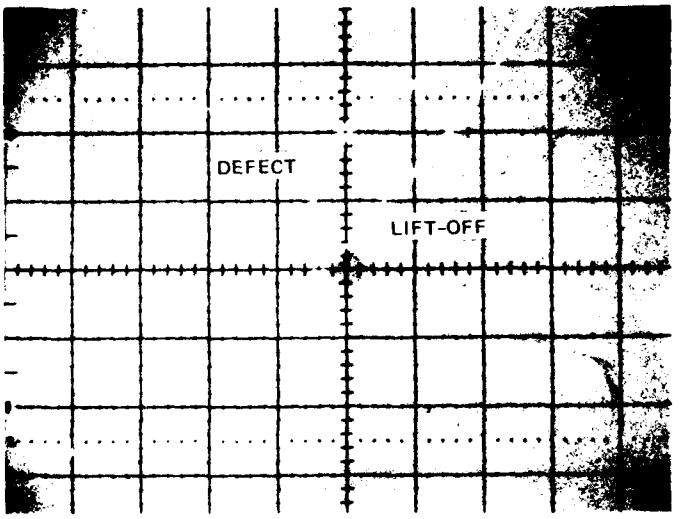

(a) ALUMINUM CALIBRATION PLATE, SLOT 3

DISPLAY SENSITIVITY = 2.0 V/div (both axes)

DEFECT SENSITIVITY ~ 6 V

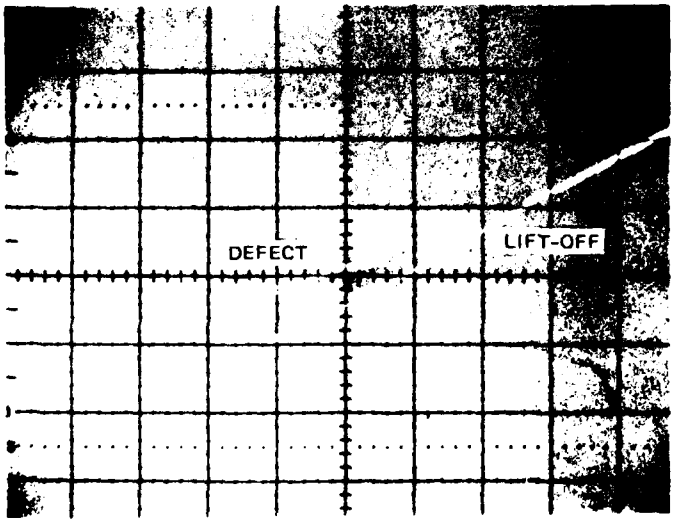

(b) TITANIUM PLATE, SLOT C

DISPLAY SENSITIVITY = 0.5 V/div (both axes)

DEFECT SENSITIVITY ~ 0.8 V

FIGURE A-17 RESPONSES OF FLOPPY-DISK PROBE TO SHALLOW EDM SLOTS

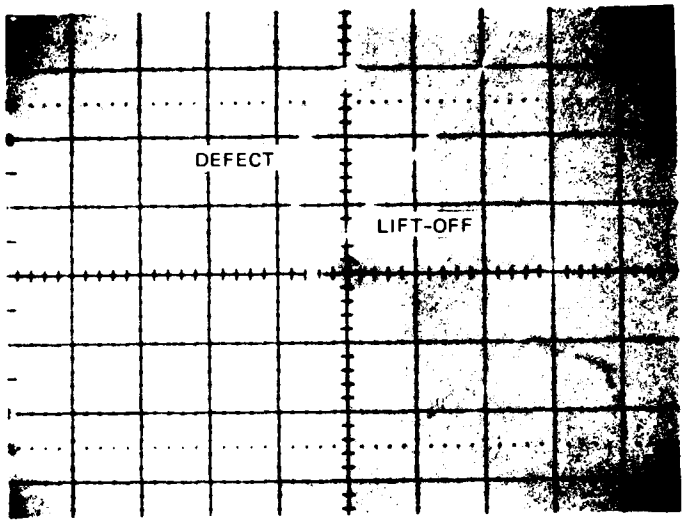

(a) 2024-T3 ALUMINUM, SAMPLE B3

DISPLAY SENSITIVITY = 2 V/div (both axes)

DEFECT SENSITIVITY ~ 6 V

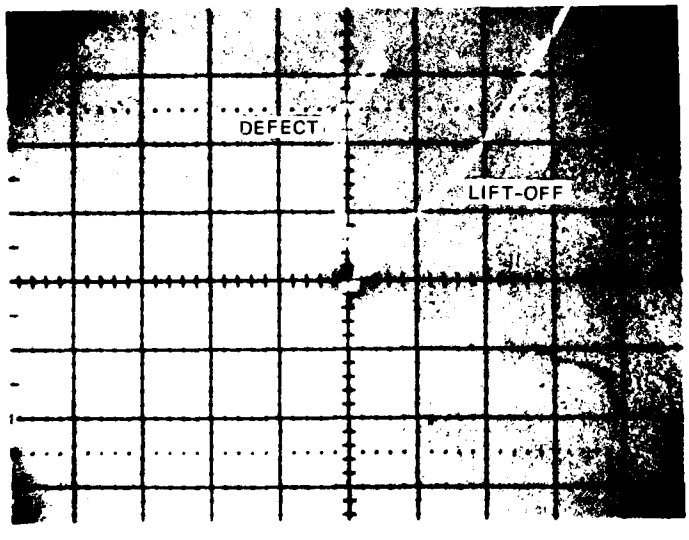

(b) 2024-T3 ALUMINUM, SAMPLE C3

DISPLAY SENSITIVITY = 2 V/div (both axes)

DEFECT SENSITIVITY ~ 6.4 V

FIGURE A-18 RESPONSES OF FLOPPY-DISK PROBE TO CLOSED FATIGUE CRACKS

9. Lift-Off Measurements

In order to quantify the effects of changes in probe-to-sample spacing (lift-off), the mechanical scanning stage was mounted on a 1-in.-thick aluminum jig plate, and four dial indicators with resolutions of 0.0001 in. were incorporated to align the probe and sample, as well as to measure the probe-to-sample spacing. This mechanical arrangement was described in Section III-B.

Microwave probe 2, because of its high sensitivity to shallow EDM slots, was chosen to be characterized. The smallest EDM slot on a flat plate (titanium sample, slot D) was used as the reference flaw in order to avoid saturating the measurement system at the smallest probe-to-sample spacing of interest. The results of this measurement are shown plotted in Figure A-19. These results are shown separately for each of the two probes (A and B) that make up the differential system.

It was found that the tolerances maintained during the assembly of this prototype differential probe resulted in probe B being recessed below the wear plate. Hence, probe B was 0.0015 in. further from the sample. This difference in probe-to-sample spacing resulted in the maximum signal from probe A being about twice as large as that produced by probe B. We concluded from this result that a good deal of care will be needed during assembly of the differential system so that both probes are even with the wear plate.

Another very interesting characteristic is apparent in Figure A-19, in which it is shown that the signal from each probe initially increased as probe-to-sample spacing was increased, then reached a maximum before decreasing. This behavior is probably caused by mutual coupling between the probes.

For purposes of comparison, the lift-off sensitivity of the commercial differential probe (SP/DP-100) was measured for a slot and a closed crack. Slot E in the titanium plate was chosen for this purpose because of the probe's limited sensitivity to shallow EMD slots. The maximum

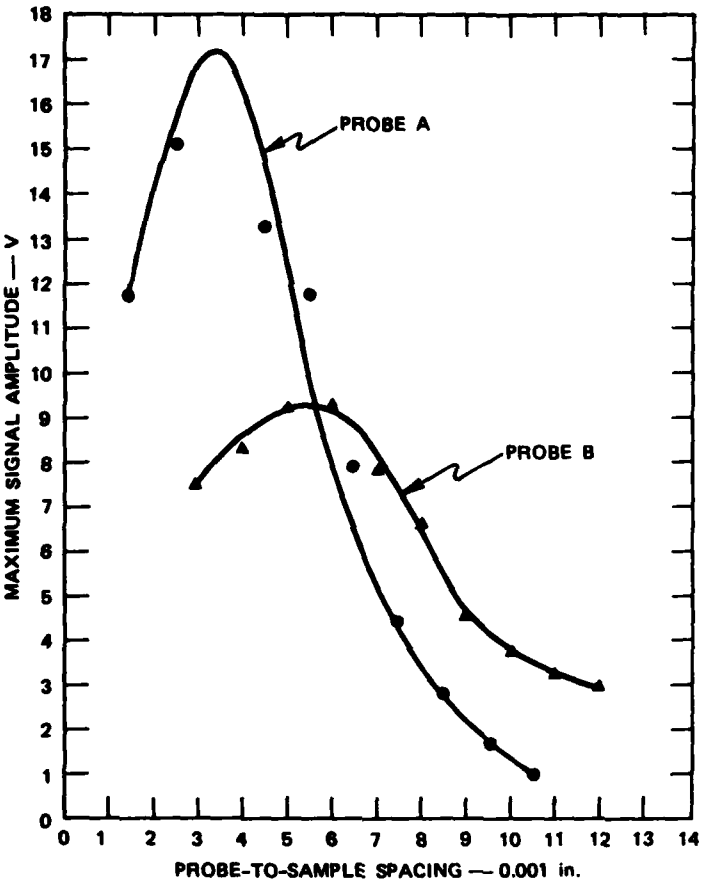

FIGURE A-19 MEASURED LIFT-OFF SENSITIVITY OF PROTOTYPE MICROWAVE EDDY-CURRENT PROBE 2

signal amplitude is shown as a function of probe-to-sample spacing in Figure A-20 for both flaws. In order to facilitate the comparison with the microwave probe, the data have been normalized and combined, as shown in Figure A-21. These data show that the microwave probe is more sensitive to lift-off than the lower-frequency commercial probe. We believe that this behavior is more a result of differences between the geometries of the probes, and less a result of differences in the operating frequency.

10. Annular-Ring Measurements

The most promising of the experimental probes were configured as hole-inspection probes and used to scan the shallow EDM slot in the

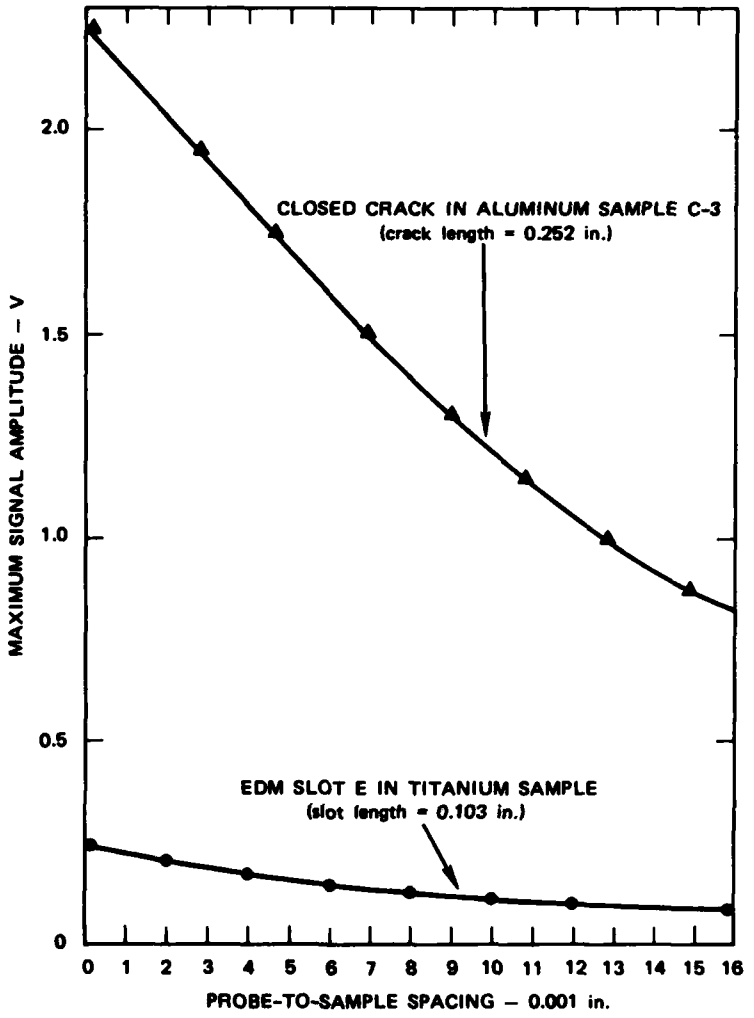

FIGURE A-20 MEASURED LIFT-OFF SENSITIVITY OF 100-kHz DIFFERENTIAL PROBE (NORTEC SP/DP-100)

titanium split annular ring. The probes tested in this way were:

- Microwave probe 2 (differential probe)
- Printed-coil probe (absolute probe)
- Floppy-disk probe (absolute probe).

For comparison purposes, the commercial hole-inspection probe (DP-64) was also used, but it was not able to detect the flaw for the signal levels used.

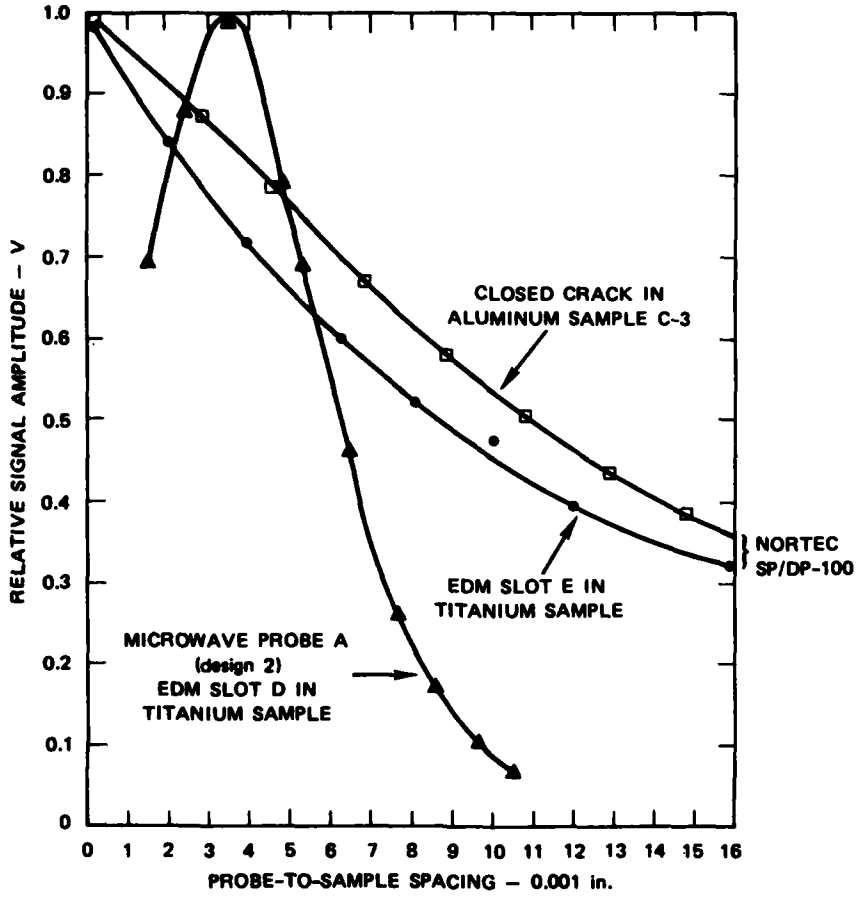

FIGURE A-21 NORMALIZED LIFT-OFF SENSITIVITY FOR 100-kHz AND MICROWAVE DIFFERENTIAL PROBES

The measured responses for these probes are shown in Figure A-22. The microwave probe demonstrated ample defect sensitivity (about 20 dB greater than the printed-coil probe). The floppy-disk probe displayed marginal sensitivity (about 20 dB less than the printed coil probe). The lift-off discrimination for the microwave probe was poor. On the other hand, both the printed-coil probe and the floppy-disk probe produced flaw signals which were orthogonal to the lift-off signals. However, it was still easier to detect the small slot with the microwave probe because its response was so much larger.

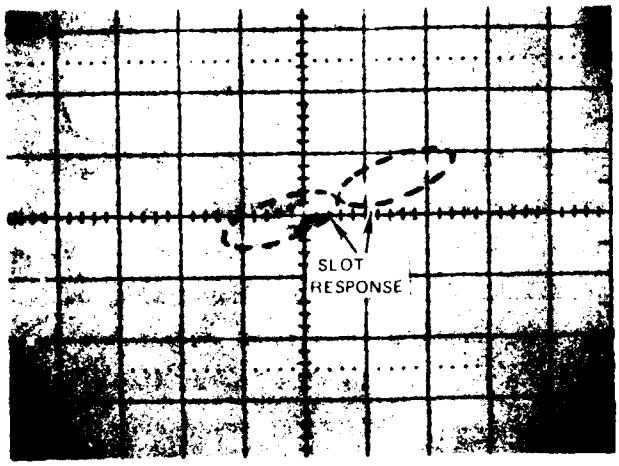

(a) MICROWAVE PROBE 2

DISPLAY SENSITIVITY = 1 V/div (both axes)

DEFECT SENSITIVITY ~ 1.6 V

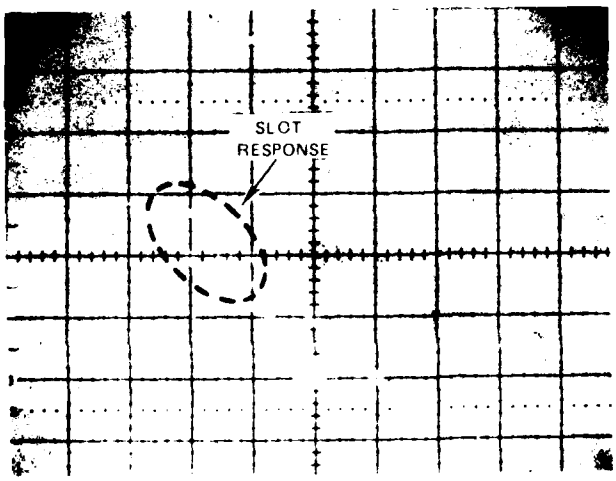

(b) PRINTED-COIL PROBE

DISPLAY SENSITIVITY = 0.2 V/div

DEFECT SENSITIVITY ~ 0.2 V

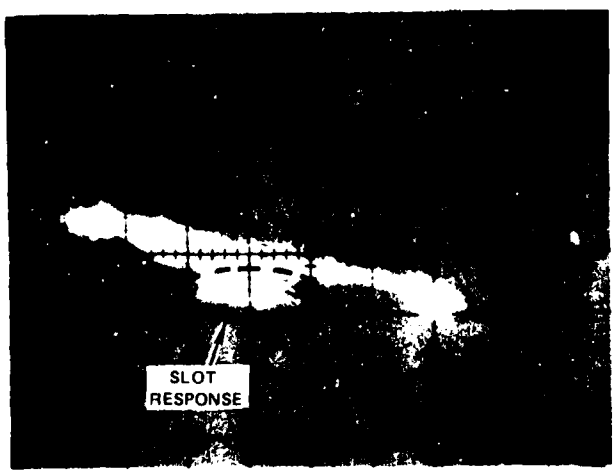

(c) FLOPPY-DISK PROBE

DISPLAY SENSITIVITY = 0.05 V/div (both axes)

DEFECT SENSITIVITY ~ 0.03 V

FIGURE A-22 RESPONSES OF VARIOUS PROBES TO A SHALLOW EDM SLOT IN THE TITANIUM ANNULAR RING

C. Reproducibility Demonstration

1. Printed-Coil Probe

Five printed-coil probes were fabricated and used to scan the shallow EDM slot in the annular ring in order to demonstrate the reproducibility of the probe response. Figure A-23 shows the measured input impedances of the five probes at 125 MHz. The data are displayed on a 50-Ω Smith chart. In air, the impedances of all five probes are identical to within the resolution of the chart. However, when the probes were placed in the annular ring, the measured input impedances varied by about ±10 percent, indicating a variation in lift-off between the different probes.

A typical lift-off/background signal produced by rotating the sample while the probe was located in a flaw-free region is shown in Figure A-24. The small excursions from a straight line are thought to be caused by the shallow tool marks on the surface of the hole.

The appearance of the flaw signal as displayed on the storage oscilloscope varied from probe to probe. A set of typical displays is shown in Figure A-25. This variation in response appeared to be due primarily to small variations in probe-to-sample contact pressure during the manual scan. However, the defect sensitivity (defined as the maximum trace excursion orthogonal to the trace produced by lift-off) showed reasonable reproducibility. The shallow EDM slot was scanned with each of the five probes on three different days to establish the reproducibility of data for a given probe, as well as the reproducibility between probes. The results of these measurements are summarized in Table 1 in Section III-E.

2. Microwave Probe

The reproducibility of the microwave probe was evaluated by fabricating two sets of the printed-circuit boards that comprise microwave probe 2, and then using each set in conjunction with a single probe housing and RF bridge to scan the shallow EDM slot in the annular ring.

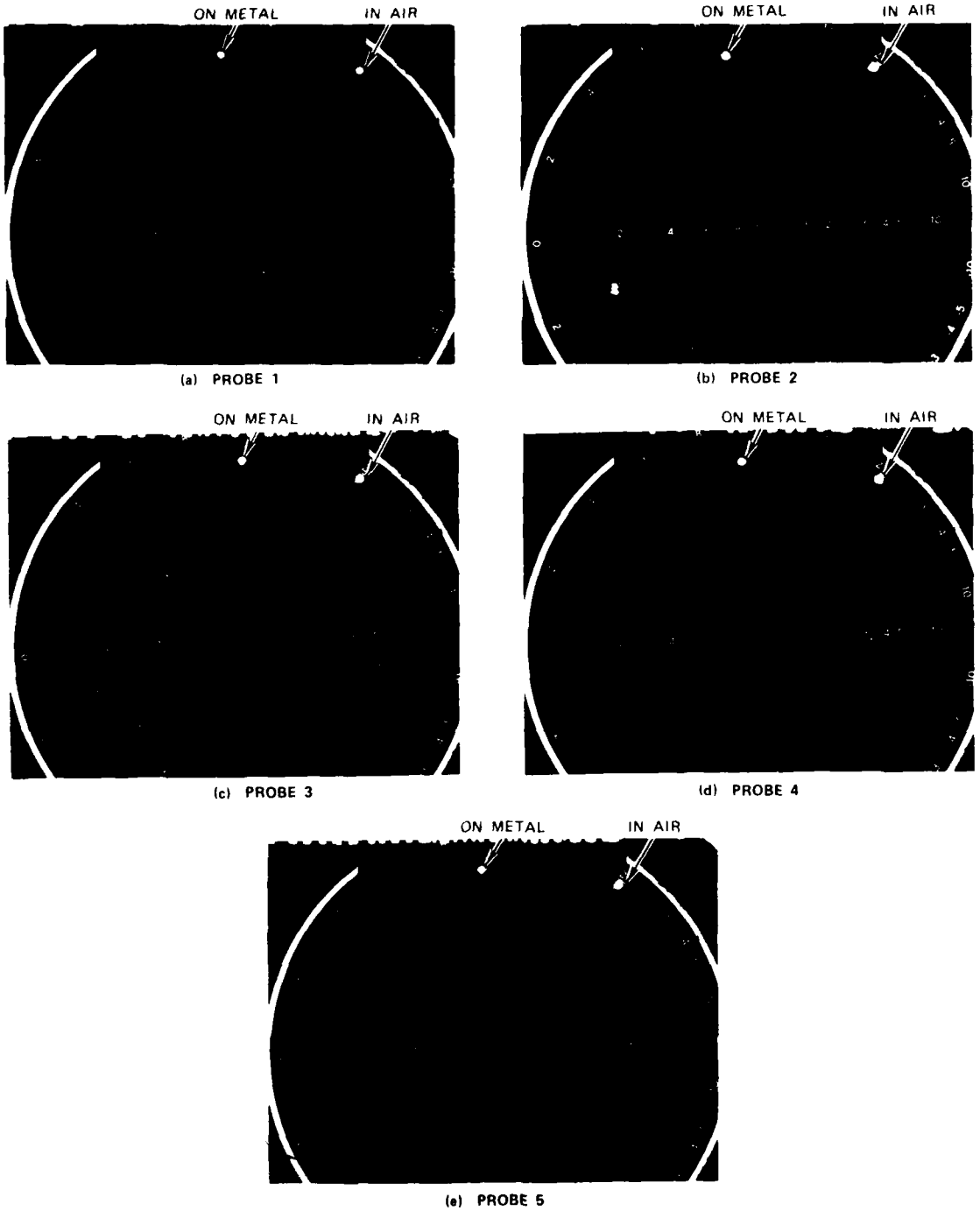

FIGURE A-23 INPUT IMPEDANCES OF FIVE DIFFERENT PRINTED-COIL PROBES AT 125 MHz

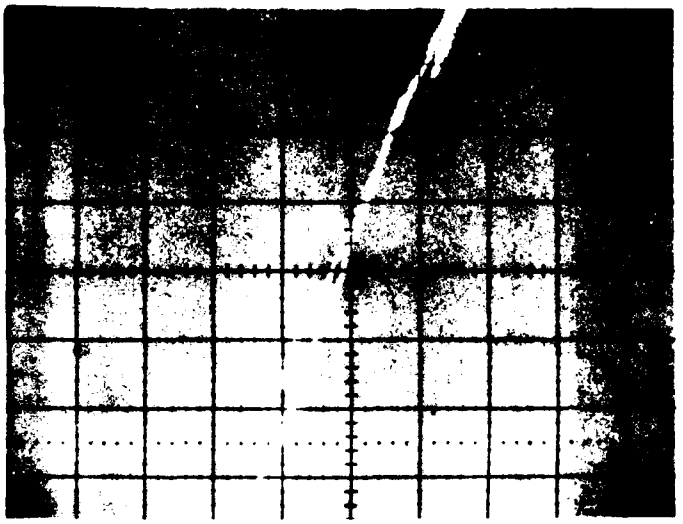

DISPLAY SENSITIVITY = 0.2 V/div
(both axes)

FIGURE A-24 TYPICAL LIFT-OFF/BACKGROUND SIGNAL FOR A PRINTED-COIL PROBE

The resulting responses of the two microwave probes are shown in Figure A-26. Probe 2A produced a relatively symmetrical response, as is characteristic of a differential probe. The corresponding defect sensitivity was 3.3 V. On the other hand, the response of probe 2B was unsymmetrical, and the defect sensitivity was only 1.6 V. In an effort to explain this variation between the two probes, the probe dimensions were measured using a microscope. It was determined that the 0.010-in.-wide strip that short-circuits the microstrip to the ground plane was recessed about 0.005 in. more in the less sensitive probe than the other. In addition, the short-circuiting strip in the less sensitive probe was shifted laterally by nearly 0.002 in. This mechanical asymmetry produces an electrical asymmetry in the coupling between the flaw and the two short-circuiting strips that comprise the differential probe. As a result, this probe behaved more like an absolute probe, with only about half the defect sensitivity of probe 2A.

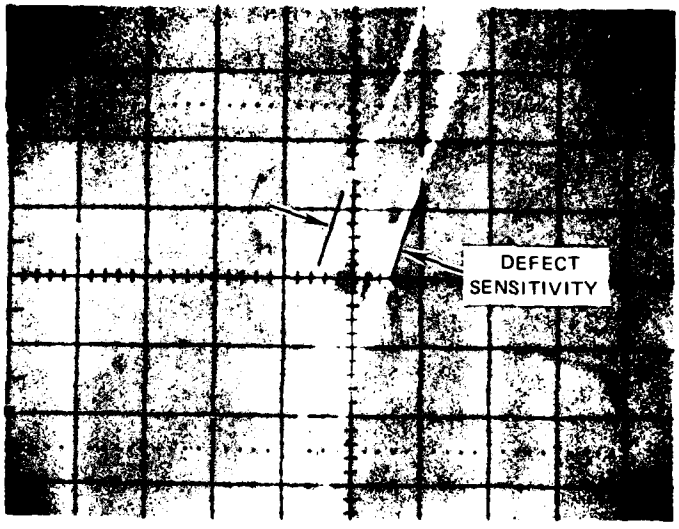

(a) **PROBE 1**

DISPLAY SENSITIVITY = 0.2 V/div
(both axes)

DEFECT SENSITIVITY = 0.2 V

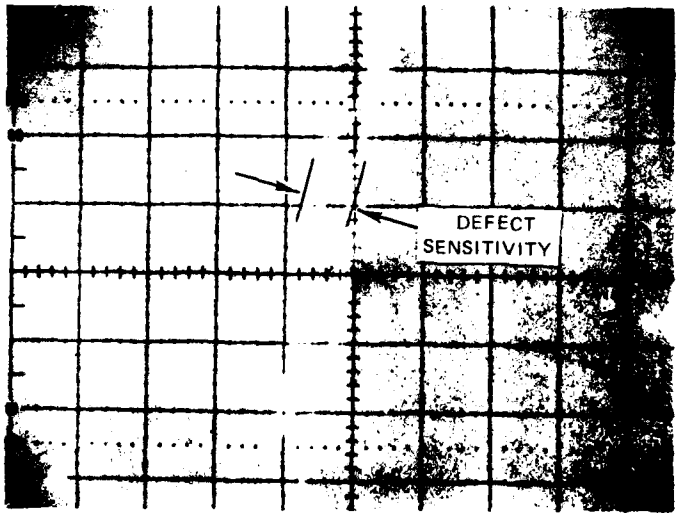

(b) ***PROBE 2***

DISPLAY SENSITIVITY = 0.2 V/div
(both axes)

DEFECT SENSITIVITY = 0.15 V

FIGURE A-25 REPRESENTATIVE RESPONSES OF FIVE PRINTED-COIL PROBES TO THE EDM SLOT IN THE TITANIUM ANNULAR RING

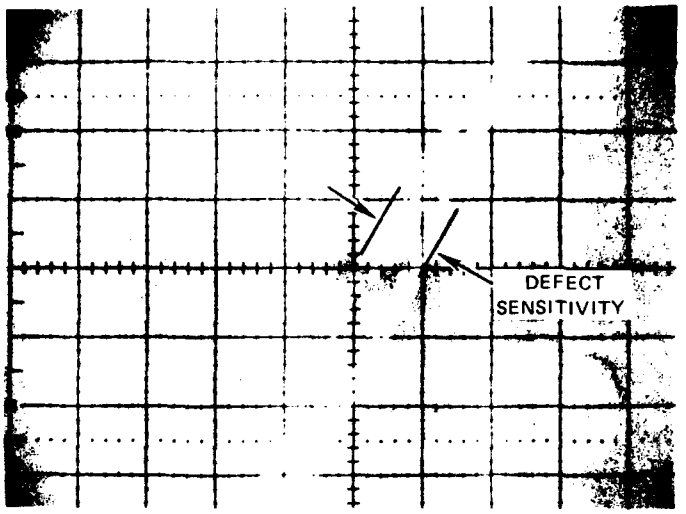

(c) PROBE 3

DISPLAY SENSITIVITY = 0.2 V/div (both axes)

DEFECT SENSITIVITY = 0.16 V

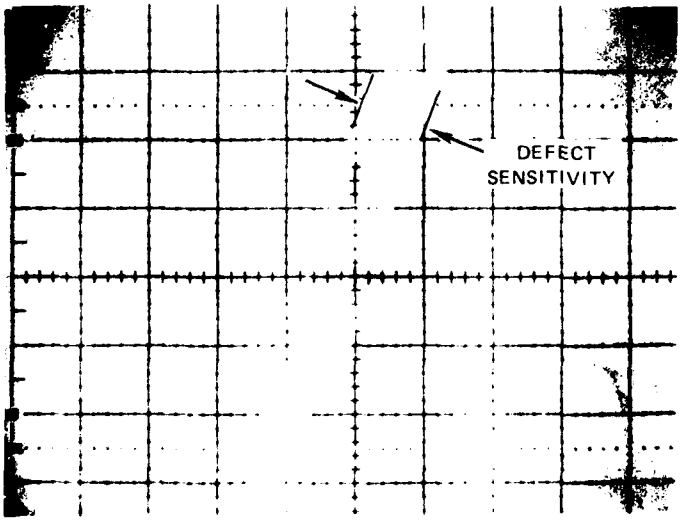

(d) PROBE 4

DISPLAY SENSITIVITY = 0.2 V/div (both axes)

DEFECT SENSITIVITY = 0.18 V

FIGURE A-25 (CONTINUED)

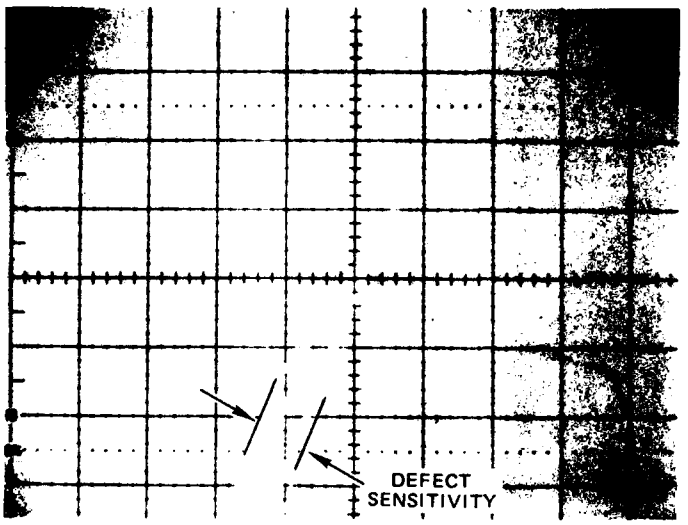

(e) PROBE 5

DISPLAY SENSITIVITY = 0.2 V/div (both axes)

DEFECT SENSITIVITY = 0.16 V

FIGURE A-25 (CONCLUDED)

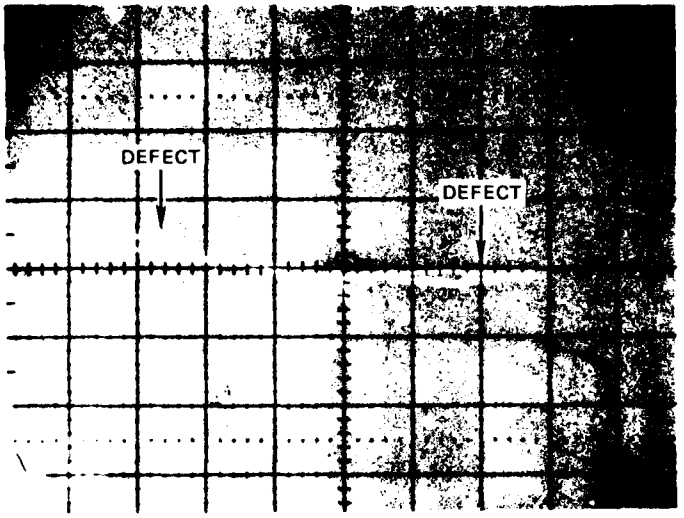

(a) PROBE 2A

DISPLAY SENSITIVITY = 0.5 V/div (both axes)

DEFECT SENSITIVITY = 3.3 V

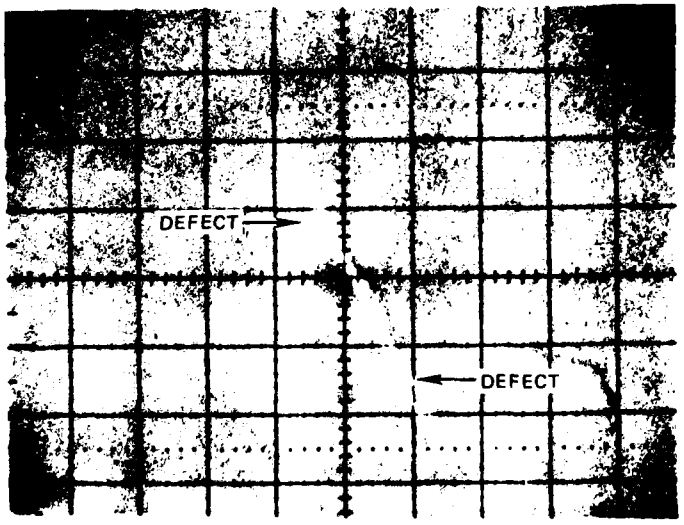

(b) PROBE 2B

DISPLAY SENSITIVITY = 0.5 V/div (both axes)

DEFECT SENSITIVITY ~ 1.6 V

FIGURE A-26 RESPONSES OF TWO MICROWAVE PROBES TO THE EDM SLOT IN THE TITANIUM ANNULAR RING

REFERENCES

1. S. Ramo and J. R. Whinnery, Fields and Waves in Modern Radio, New York: John Wiley and Sons, pp. 259-262 (1956).

2. R. E. Collin, Field Theory of Guided Waves, New York: McGraw-Hill, pp. 39-40 (1960).

3. B. A. Auld, "Theory of Ferromagnetic Resonance Probes for Surface Cracks in Metals," G. L. Report 2839, Ginzton Laboratory, Stanford University, Stanford, California (July 1978).

4. B. A. Auld, "Theoretical Characterization and Comparison of Resonant-Probe Microwave Eddy-Current Testing with Conventional Low-Frequency Eddy-Current Methods," Eddy Current Characterization of Materials and Structures, ASTM STP 722, G. Birnbaum and G. Free, eds., American Society for Testing and Materials, pp. 332-347 (1981).

5. M. L. Burrows, "A Theory of Eddy-Current Flaw Detection," University Microfilms, Inc., Ann Arbor, Michigan (1964).

6. C. V. Dodd, "Solutions to Electromagnetic Induction Problems," ORNL-TM-1842 (1967) and Ph.D. Dissertation, the University of Tennessee (1967).

7. C. V. Dodd and W. E. Deeds, "Analytical Solutions to Eddy-Current Probe-Coil Problems," Journal of Applied Physics, Vol. 39, pp. 2829-2838 (May 1968).

8. C. V. Dodd, W. E. Deeds, and J. W. Luquire, "Integral Solutions to Some Eddy-Current Problems," International Journal of Nondestructive Testing, Vol. 1, No. 1, pp. 29-90.

9. J. W. Luquire, C. V. Dodd, W. E. Deeds, and W. G. Spoeri, "Computer Programs for Some Eddy-Current Problems" ORNL-TM-2501 (August 1969).

10. T. G. Kincaid et al., "Two Approaches to Solving the Inversion Problem for Eddy-Current NDE," Proceedings of the DARPA/AF Review of Progress in Quantitative NDE, La Jolla, California (July 1979).

11. T. G. Kincaid, K. Fong, and M. V. K. Chari, "Progress in Solving the Three-Dimensional Inversion Problem for Eddy-Current NDE," Proceedings of the DARPA/AF Review of Progress in Quantitative NDE, La Jolla, California (July 1980).

12. R. Palanisamy and W. Lord, "Finite Element Modeling of Electromagnetic NDT Phenomena," IEEE Transactions of Magnetics, Vol. MAG-15, No. 6, pp. 1479-1481 (November 1979).

13. W. Lord, "Development of a Finite Element Model for Eddy-Current NDT Phenomena," Review of Progress in the EPRI Program in NDE&E, Special Report, Electric Power Research Institute, Palo Alto, California (October 1980).

14. A. J. Bahr, "Using Electromagnetic Scattering to Estimate the Depth of a Rectangular Slot," IEEE Transactions on Antennas and Propagation, Vol. AP-27, pp. 738-746 (November 1979).

15. A. J. Bahr, "Microwave Eddy-Current Techniques for Quantitative Nondestructive Evaluation," Eddy-Current Characterization of Materials and Structures, ASTM STP 722, G. Birnbaum and G. Free, eds., American Society for Testing and Materials, pp. 311-331 (1981).

16. R. E. Beissner, C. M. Teller, F. L. Burkhardt, R. T. Smith, and J. R. Barton, "Detection and Analysis of Electric Current Perturbations Caused by Defects," Eddy-Current Characterization of Materials and Structures, ASTM STP 722, G. Birnbaum and G. Free, eds., American Society for Testing and Materials, pp. 428-446 (1981).

17. W. D. Dover, F. D. W. Charlesworth, K. A. Taylor, R. Collins, and D. H. Michael, "The Use of ac Field Measurements to Determine the Shape and Size of a Crack in a Metal," Eddy-Current Characterization of Materials and Structures, ASTM STP 722, G. Birnbaum and G. Free, eds., American Society for Testing and Materials, pp.401-427 (1981).

18. B. A. Auld, F. Muennemann, and D. K. Winslow, "Surface Flaw Detection with Ferromagnetic Resonance Probes," Proceedings of the DARPA/AF Review of Progress in Quantitative NDE, La Jolla, California (July 1980).

19. B. A. Auld, F. Muennemann, and D. K. Winslow, "Observation of Fatigue Crack Closure Effects with the Ferromagnetic Resonance Eddy-Current Probe," G. L. Report 3233, Ginzton Laboratory, Stanford University, Stanford, California (March 1981).

*U.S.Government Printing Office: 1982 — 559-006/5056


DATE
ILMED
4-8